Experimental study of enhancement techniques used in the volume-production-type negative hydrogen ion source

Makoto Hamabe

DOCTOR OF PHILOSOPHY

Department of Fusion Science

School of Mathematical and Physical Science

The Graduate University for Advanced Studies

1997

Abstract

The developments of large current negative hydrogen / deuterium ion (H^- / D^-) source using the volume production method have succeeded enough to be utilized for the NBI in the thermonuclear fusion research. This enhancement of H^- beam current is achieved by using several empirical techniques. However, the physical process in the ion source has not been examined in detail, so that we don't have a clear image on production and extraction of negative ions in and from plasma.

In order to develop more efficient ion source, i. e., to extract higher current density applying for the NBI, it is important to know what happens in plasma according to these empirical techniques, especially in the present "large current" negative ion source. In this work, the characteristics of H^- and electrons in the extraction region of the plasma source is studied and compared with extracted H^- and electron beam comprehensively. For this sake, the NIFS 1/6 scale negative ion source, which had been used for R&D, was modified to use an external magnetic filter and to have a pair of windows for the observation of the extraction region 15 mm apart from the plasma grid. From these windows, a high power laser beam is introduced, and H^- density is measured by the laser photodetachment method. Electron density and temperature are also measured by the same Langmuir probe as used in the photodetachment method. The extracted H^- beam is measured by the Faraday cup array installed 20 cm downstream from the extraction system. The extracted electron current is obtained from the drain current of the extraction power supply.

The effects of three empirical techniques are examined; (1) magnetic filter strength on the

extraction region, (2) cesium vapor injection into the arc chamber, (3) addition of bias voltage to the plasma grid against the arc chamber.

It is generally reported that the magnetic filter strength is enough if the electron temperature is suppressed less than 1 eV in the extraction region to avoid the destruction of H^- by the collision with the high energy electrons. But it is not the case of our study. Even if the electron temperature is below 1 eV, there still remains a high energy component in the energy distribution of electrons. In this case, the extracted H^- current as well as H^- density in the extraction region is small at the high arc power discharge. With the stronger filter field, a high energy component of electrons is decreased, and then destruction of H^- ions at a high arc power is sufficiently suppressed. Hence, in the design of the H^- ion source, it is important to decide the magnetic filter field so as to suppress the high energy electrons sufficiently.

Under the pure volume discharge, it is observed that both extracted H^- and electron currents are proportional to the H^- and electron densities in the extraction region. After the cesium injection, extracted H^- current increases about twice while the electron current reduces an order of magnitude, which are the common effects observed in other ion sources as well. In the extraction region plasma, however, H^- density increases by $5 \sim 10$ times while the electron density reduces only by half. The linearity between the extracted current and the density in the plasma still holds in the cesiated discharge, but the coefficient is different from that of the pure volume discharge. The electron temperature becomes slightly lower after cesium injection. The difference of coefficient of H^- current to its density is considered to come from the difference of H^- temperature. If we assume that the thermal ion flux determines the extraction current density, the temperature of H^- is estimated about 0.3 eV in the pure

volume discharge, and 0.07 eV in the cesiated discharge.

The bias voltage dependence shows that the extracted electron current sharply decreases when the applied voltage becomes more positive but that the electron density in the extraction region does not vary. On the other hand, H^- current shows the same behavior as H^- density in plasma. Therefore the extracted electron current reflects the electron density in the vicinity of plasma grid, where the electron density becomes very small after cesium injection and is sensitive to the potential between the plasma grid and the plasma.

The addition of cesium in the volume-production-type ion source enhances the H^- production more remarkably than expected from extracted beam current. On the other hand, the electron density and the temperature do not change much. These results can not be explained by the volume process alone. The fact that the extracted electron current decreases much in the cesiated discharge shows that the electron density in the vicinity of plasma grid is very low, which suggests the surface production of H^- ion on plasma grid. These H^- ions are not extracted directly from the originated region but they are accelerated by a potential between the grid and plasma and go through the extraction region affecting by magnetic filter field and collision before extracted from the grid aperture. However, the other fact that the H^- is still observed at the highly positive bias voltage means that the volume production also remains.

Experimental study of enhancement techniques used in the volume-production-type negative hydrogen ion source

Contents

A	Amplitude of Gaussian profile
a	Radius of a beam
c	Speed of light
e	Charge of electron
H	Height of plasma source
h	Planck's constant
I_{ext}	Extraction current on extraction voltage source
I_{H^-}	H^- beam current
I_{es}	Electron saturation current on a Langmuir probe
I_{pe}	Electron current flowing into a Langmuir probe
I_{pe0}	I_{pe} when $V_{probe} = V_p$
$J(\ )$	Radial H^- beam current density
J_{H^-}	H^- beam density through a plasma grid aperture
L	Length og plasma source
M	Rest mass of H^-
N_e	Electron density
N_{e0}	Electron density of main part of two component electrons
N_{e1}	Electron density of high temperature part of two component electrons
N_{H^-}	H^- density
S	Surface area of a Langmuir probe
T_e	Electron temperature (in eV)
T_{e0}	Electron temperature of main part of two component electrons
T_{e1}	Electron temperature of high temperature part of two component electrons
V_p	Plasma potential
V_{probe}	Voltage applied on a Langmuir probe
v	Speed of a beam
x	Horizontal variable

x_0	Horizontally center position of a H^- beam
β	$= v/c$
ΔI^-	Photodetachment signal
ΔN_{H^-}	Photodetached H^- density
ε	Emittance
ϕ	Diameter of plasma source
ν	Frequency of a laser light
$\ln \Lambda$	Coulomb logarithm
σ	Cross-section
λ_{ii}	Mean free path for the Coulomb collision
υ''	State number of vibrationally excited hydrogen molecule
ω	Dispersion of Gaussian profile
$\ln \Lambda$	Coulomb logarithm

1. Introduction

1-1. The development of the large size negative hydrogen ion sources for negative-ion-based neutral beam injection

Neutral beam injection (NBI) is one of the reliable methods for the plasma heating and the current drive for nuclear fusion experimental devices. As the sizes of the devices are larger for the nuclear fusion reactor research, required neutral beam energy is higher so as to heat the central part of plasma sufficiently. For example, the International Thermonuclear Experiment Reactor (ITER) is designed to require 1 MeV neutral beam[1]. However, the positive hydrogen ion sources which are usually used for the present NBI cannot be used in such high energy region because the neutralization efficiency from positive hydrogen ion (H^+) or positive deuterium ion (D^+) to neutral hydrogen atom (H^0) or neutral deuterium atom (D^0), respectively, reduces to nearly zero[2]. On the other hand the neutralization efficiency from negative hydrogen ion (H^-) or negative deuterium ion (D^-) to H^0 or D^0, respectively, saturates at 60 % even in high energy region[2]. That is why the negative-ion-based NBI (N-NBI) is essentially required for the heating of the enlarged plasma devices.

The developments of large H^- / D^- sources for the N-NBI have been advanced with adopting the technology of intensive small-sized negative ion sources[3] and have succeeded in the production of large current over 10 A and high energy H^- / D^- beam[4][5]. At JT-60U in Japan Atomic Energy Research Institute (JAERI), 500 keV N-NBI heating

experiment has started[6].

The N-NBI system is to be utilized also on the Large Helical Devices (LHD) which is under construction in the National Institute for Fusion Science (NIFS). The system contains four negative ion sources designed to produce a H^- beam of 180 keV / 40 A [7]. To realize such large ion sources, 1/6-scaled and 1/3-scaled sources were developed and had proved their preferable capability[8][9]. Based on these results, test of the real-sized ion sources for the LHD-N-NBI has already started[10].

Table 1-1 shows the development of large current or high energy H^- sources and their application. Compared with other H^- sources, such as for accelerator, H^- sources for N-NBI must produce large current beam with large area. That is because high power of tens MW is necessary to heat plasma in the nuclear fusion devices which have large volume plasma. For this purpose, it is necessary in the N-NBI field to develop large current H^- sources, because the optimum beam energy is determined by other conditions. So far, the current density of negative ion is an order of magnitude smaller than that of positive ion,

Site	Size	Beam current	Current density	Beam energy	Application
LBL [3]	ϕ 7.5cm x H 8 cm	150 mA	1200 mA/cm^2	16 keV	R&D
Ecole polytechnique [11]	ϕ 44 cm x H 45 cm	0.7 mA	1.4 mA/cm^2	2 keV	R&D
JAERI [6]	ϕ 64 cm x L 122 cm semicylindrical	13.5 A (D^-)	8.1 mA/cm^2	400 keV	N-NBI
NIFS [9]	35 cm x 62 cm x H 20 cm rectangular	16.2 A	31 mA/cm^2	125 keV	N-NBI
KEK [12]	ϕ 10 cm x H 16 cm	20 mA	45.5mA/cm^2	30 ~ 40 keV	Accelerator

Table 1-1. Large current / high energy H^- / D^- volume sources.

which means that the negative ion source becomes very large. High current density is then required to reduce the size of ion source. The production of uniform beam in such a large ion source is other problem.

1-2. Enhancement of the performance of the negative ion source

In the development of H^- sources for N-NBI, in this decade, three kinds of the techniques were developed to enhance the performance of the H^- source; (1) use of the tandem source equipped with magnetic filter in the arc chamber, (2) injection of cesium into the arc chamber and (3) supply of the bias voltage between the arc chamber and the plasma grid. They are described here briefly. These three techniques are also examined in this work.

1-2-1. The tandem source

As will be described in the section 2-1, high energy electrons ($\geq$ 40 eV) and low energy electrons ($\sim$ 1 eV) are considered necessary to produce H^- ions by the volume production process. The "tandem" source has two regions in the plasma separated by the weak magnetic field. The electron temperature is different in these regions; one is low temperature region called "extraction region" and another is high temperature region called "driver region" (Fig. 1-1).

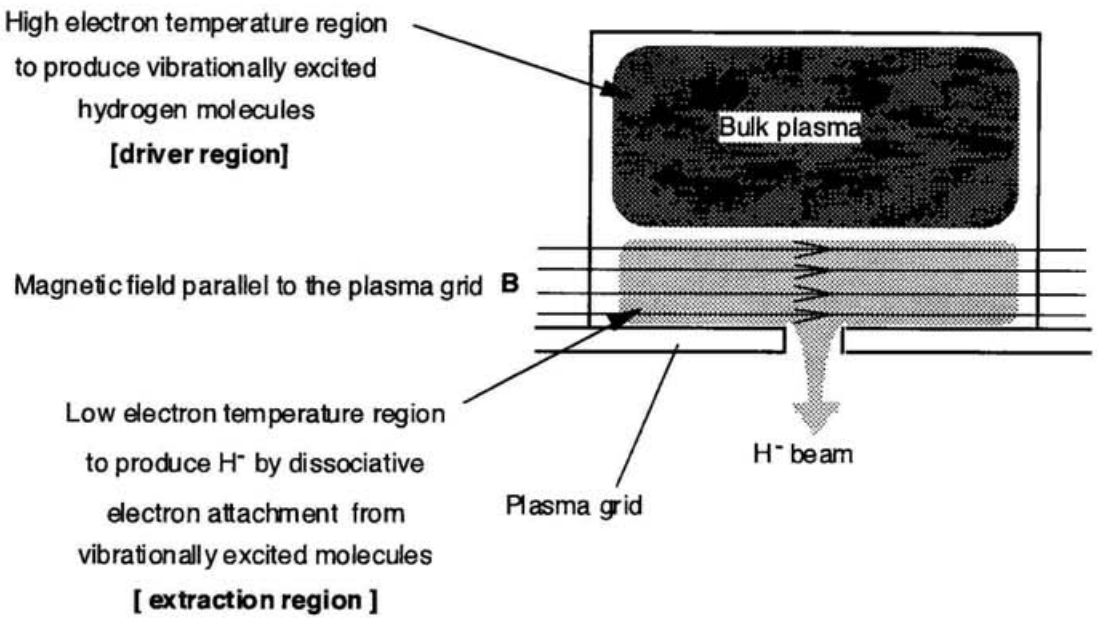

Fig. 1-1 An illustration of the tandem source.

In early days, the magnetic field for the tandem source was equipped by the permanent magnet rods inserted in the arc chamber[13], which is called the rod filter. However, the rod filter has a disadvantage that the magnet rods cause the increase of the plasma loss area. Presently, the external filter is usually used, which is produced by the pair of strong magnets placed on the plasma grid outside of the extraction region[14]. The Plasma Grid (PG) filter, which uses transverse magnetic field produced by the current across the plasma grid, is also used for the JT-60 N-NBI[6] and proposed for the ITER[1] in addition to the external filter. This type of ion source is easily scaled up at least in one direction so that large current can be expected. Also from technical point of view, this ion source is similar to the conventional positive ion source. By these reasons, this type of ion source has become "standard" as the negative ion source for N-NBI.

1-2-2. Cesium vapor injection into the arc chamber

Walther et al. showed the remarkable improvement of the ion source performance by injection of cesium in their small H^- source[15]. After that in the case of the larger H^- source, this improvement of the performance is also ensured, i. e., the extracted H^- beam current is multiplied and the electron current extracted simultaneously with H^- is substantially suppressed[3][4][9]. To clarify the physical process of the effect of this cesium vapor is the most intensively discussed problem in the field of the H^- source engineering. As the effect of cesium on the process for the H^- formation in the ion source, three physical processes through the volume processes or the surface processes are proposed[15].

(1) Electron cooling is caused by the diffusion of low energy electrons across the magnetic filter field with the massive cesium ions.

(2) Vibrational excitation of the hydrogen molecule is enhanced by the reaction between cesium atom and H_3^+ ion.

(3) Surface production of H^- is improved by the decrease of the work function of the plasma grid surface.

Details of them are treated in the section 2-3.

1-2-3. Bias voltage to the plasma grid

Leung et al. found that supply of the bias voltage to the plasma grid against arc chamber had the effect of reduction of the extracted electron current, using the small ion source[13]. This suppression is also observed in the large H^- source for the N-NBI. Too high bias voltage suppresses even the H^- current. At the optimum voltage, however, electron current is suppressed sufficiently with little decrease of the H^- beam current. The effect of this bias supply is explained by the $\boldsymbol{E} \times \boldsymbol{B}$ drift due to the electric field of bias potential and by the magnetic field of the magnetic filter[13], but this model is doubtful because the behavior of the plasma particle in the extraction region to the bias voltage is not clearly studied, except for the case of the hybrid multicusp source by Bacal et al. [11][16]-[19]. The bias characteristics of the H^- density and the electron density in the extraction region are measured and compared with those of the H^- beam extraction in this work.

1-2-4. What happens in the ion source under these enhancement techniques?

These techniques used to improve high performance sources have left us the interesting and challenging problems in the view of the plasma physics, i. e., it is not explained clearly how such large H^- current is formed in and extracted from an ion source. Although engineering of H^- ion sources has established the techniques, which are

described above, in order to enhance the performance of H^- sources, their physical understanding is still poor.

There are several works to predict the characteristics of the ion source plasma by means of numerical simulation in order to know the H^- formation processes in the ion source[20]-[22], but there is not enough experimental data from actual H^- sources to prove the accuracy of these calculations. The relation between the behavior of H^- ions in an ion source and extracted H^- beam is not examined well in actually designed H^- sources, although it is important to consider, for example, the sheath problem on the boundary of the plasma in the extraction region to develop the simulation code of H^- beam orbit. Therefore it is significant to research this relationship in the H^- sources, which is similar to the ion sources used in N-NBI, experimentally for clarifying which physical processes contribute to the enhancement of the H^- formation.

Measurements of the ion source plasma have been energetically done by Bacal et al. with using the "Camembert" ion sources[11][16]-[19]. They have measured and discussed characteristics of the electrons and H^- ions in the plasma by the photodetachment method. They especially give the weight to the bias voltage effect on the plasma grid. Formerly they used the medium-sized H^- generator, named "Camembert II", and measured the H^- density by the photodetachment method[16]. Its characteristics were compared to the one of the extracted H^- current in terms of their bias voltage characteristics. As the results, they proved good correspondence between them. However, enhancement of H^- production by cesium seeding was not examined in these studies. They also measured the H^- ion temperature from the relationship between the H^- density near the plasma grid and the

extracted H^- beam current, assuming that the extracted H^- beam current is equal to the thermal flux of H^- ions through the extraction aperture[17].

Then they enlarged the size of the H^- source to "Camembert III" source. Using this source, they measured the electron and H^- density and temperature[18]. In this case H^- temperature was measured by double laser method. They also extracted H^- beam from "Camembert III"[11], but its comparison to the ion source plasma still seems to be insufficient. It is true that "Camembert III" is large in scale, as shown in Table 1-1, but it is different from other large H^- sources for N-NBI research in the configuration of filaments and cusp magnetic field, which is called "hybrid multicusp" ion source[19].

In the case of a H^- source based on the general concept for N-NBI, observation of plasma in its arc chamber is still left as one of the important research programs.

1-3. The contents of this work

The main purpose of this work is to show experimentally how the techniques employed to enhance the performance of the H^- sources affect the characteristics of the plasma. In order to study the effects, the plasma parameters including the negative ion density in the extraction region are compared to the characteristics of the ion beam extracted from the ion source, *in situ*. In addition to the comparison between the beam characteristics and the plasma characteristics, namely the H^- density, in the extraction region, this work has following features;

(1) using the ion source with the arc chamber which has the large size enough to simulate the actual negative ion source developed for N-NBI, which also enables to observe the local position such as the extraction region,

(2) operating the ion source under the condition of the high H^- beam current density (about 5 mA / cm^2 / 14 kW input is achieved as maximum value.) and of the high density plasma (electron density $\sim 5 \times 10^{12}$ cm^3 and electron temperature $\sim$ 10 eV in the bulk plasma at maximum),

(3) examining the effect of cesium to the plasma in the extraction region.

Experimental results presented here directly show the relation between the extracted H^- beam and the H^- density in the extraction region. These results must be very useful as a database to consider the H^- beam formation in the ion source.

This paper consists of 6 sections; the introduction of this study is stated in this section 1. The section 2 introduces the H^- production process proposed theoretically, in the cases of the volume production and the surface production. In the section 3, the set-up for the experiments is described and the method is shown to measure the H^- density in the plasma and the H^- beam current extracted from the ion source. The following section 4 describes the results of the experiment. The summary of the measurements of the time evolution of H^- and electron densities in the extraction region are briefly described in the section 4-1. The section 4-2 deals with the effect of the strength of the filter magnetic field on the extraction region under the non-cesium operation. In the section 4-3, the results after

the injection of the cesium vapor into the arc chamber is shown and compared with the results in the section 4-2. In the section 4-4, the bias voltage dependence are dealt with in the case of the operation with cesium effect. The discussions of the experimental results are described in the section 5. The section 6 describes the conclusion of this work.

2. Theoretically predicted processes on production and destruction of H^- in the ion source

2-1. Volume production of H^-

H^- ions are mainly produced through the following two-step process in the plasma volume[23],

$$H_2 + e_f (\geq 40\,eV) \rightarrow H_2^* (\upsilon'') + e_{f'} \quad (2\text{-}1)$$

$$H_2^* (\upsilon'') + e_s (\sim 1\,eV) \rightarrow H^- + H^0 \quad (2\text{-}2)$$

Here, e_f and $e_{f'}$ mean the fast electrons and e_s means slow electron. $H_2^* (\upsilon'')$ shows the vibrationally excited molecule of the state υ''. H^0 means hydrogen atom. The process (2-1) means the production of the vibrationally excited hydrogen molecules by the collision with fast electron e_f. The vibrationally excited molecules are dissociated to H^- by the collision with slow electron e_s through the process (2-2) . This is called the dissociative attachment.

Under the situation that the plasma includes cesium atom, next process for the vibrational excitation is supposed,

$$H_3^+ + Cs \rightarrow H_2^* (\upsilon'') + H + Cs^+ \quad (2\text{-}3)$$

The main process of the destruction of H^- are the following three processes[24].

$$e_1 + H^- \rightarrow e_1 + H^0 + e_2 \quad (2\text{-}4)$$

$$H^- + H^+ \rightarrow 2H^0 \quad (2\text{-}5)$$

$$H^- + H^0 \rightarrow e + H_2^*(v'') \quad (2\text{-}6)$$

The process (2-4) means the dissociation of H^- by the collision with the electron e_1, and the cross-section for (2-4) is larger than the other processes as the energy of electron e_1 is higher than 15 eV[24]. The process (2-5) is the mutual neutralization and the process (2-6) is the associative detachment.

Generally, the H^- ion sources are equipped with the weak magnetic field in the arc chamber in front of the plasma grid of the extractor[13][14]. This magnetic field works as the high energy electron filter from the bulk plasma. In the magnetic filtered area called the "extraction region", slow electrons can penetrate only by diffusion from the bulk plasma while ions can pass freely because of the large enough Larmor radius of the ions. The purpose of the magnetic filter is this reduction of the high energy electrons in the extraction region, which enhances the process (2-2) and depresses the process (2-4) especially in the area where a H^- beam is extracted. This type of ion sources are called "the tandem source".

2-2. Surface production of H^-

H^- can be produced on the metallic surface by backscattering of hydrogen atom; H^0 and hydrogen ions; H_n^+, i. e. they inject on the surface, attain electron from it, and leave

away[25]. In these cases, an electron in the metal has to go across the potential barrier of the work function of the surface. Hence the H^- production is improved if the work function is low. To reduce the work function, alkali vapor such as cesium is usually evaporated on the metallic surface in the surface-production-type H^- source[26]. As more alkali atoms adsorb on the bare metallic surface, the work function of the surface becomes less than that of the metal. When the adsorption of alkali atom is around the half-monolayer, the work function reaches the minimum value. After the absorption is over the monolayer, the work function of the surface is equal to that of the adsorbed alkali metal. H^- surface production rate can attain its maximum value at the minimum work function. Production rate also is effected with the injection energy of H^0, H_n^+ [25].

2-3. Model of the cesium effect in the volume-production source

When the cesium vapor is added into the volume-production-type H^- source, the performances of the source is highly improved. Namely, the following three improvements are known;

(1) Increase of the extracted H^- beam current.

(2) Decrease of the drain current of the extracting power supply which means decreasing electrons extracted with the H^- beam.

(3) Reduction of the gas pressure of the ion source at which the source produce the maximum H^- current..

Here are shown three effects supposed as the effect of cesium vapor injection on the process of the H^- formation in the ion source[15].

As the effect of cesium to the process in the plasma volume, (a) electron cooling is considered. Cesium can easily be ionized in the hydrogen plasma because of its low ionizing cross section. Since a heavy cesium ion has lager Larmor radius than a hydrogen ion or hydrogen molecular ions, cesium ions can easily diffuse into the extraction region with the low energy electrons. Hence the electron temperature decreases in the extraction region, then the H^- loss by electron detachment of (2-4) is suppressed and the H^- formation by the dissociative attachment of (2-2) is improved more effectively. Another volume effect is (b) the increase of processes to create the vibrationally excited hydrogen molecule by reaction between cesium atom and H_3^+ ion, shown by (2-3).

On the other hand, as the surface process by the cesium adsorption on the chamber wall, (c) H^- surface production by H atom or positive hydrogen ion, (d) production of vibrationally excited hydrogen molecule on the surface by hydrogen molecule ion, are proposed.

Recently it have been believed in usual by most researchers of H^- ion source that the cesium effect in the volume-production-type H^- source is caused by the improvement of the surface production of H^- on the plasma grid. The work function of the pure metal surface reduces the adsorption of small amount of the alkali atoms. When the thickness of the layer of alkali atoms on the surface is less than mono-layer, the work function attains the minimum value[27]. When the metal is molybdenum, which is used for the plasma grid, and the alkali is cesium, the work function of the pure metal surface is 4.6 eV and the

minimum work function is 1.61 eV[27]. Hence steep drop of the work function of the plasma grid surface by the adsorption of the cesium atom less than monolayer causes the large increase of the surface production property of H^-. Since Mori et al. experimentally observed the decrease of H^- beam after the cleaning of the plasma grid coated with cesium by argon ion sputtering[12] and Okumura et al. also observed the dependence on temperature of the plasma grid at a few hundreds degree[4], this surface production is proposed to be the most reasonable. Namely, it is considered that the hot surface can keep the adsorption of cesium on the grid less than a monolayer. Because the adsorption energy between cesium atom and metal surface is higher than that between cesium atom-atom, cesium atoms hardly form multi-layer on the high temperature surface. Hence the work function of the plasma grid surface during the arc discharge is very low in the ion source with cesium vapor injection, compared with the one including no cesium.

Also when xenon or argon gas is introduced into the H^- volume source, increment of extracted H^- beam is observed. However its increasing rate is much smaller than in the case of cesium injection[15][28]. This result supports that the surface effect model is dominant in the cesium injected H^- source, since the work function of metal surface adsorbed by xenon is higher.

The cesium effect on the extracted beam is obvious but the effect on the plasma in the arc chamber is not examined enough. In order to make the cesium effect in the arc chamber clear, it is essential to study the plasma with / without cesium in the ion source which can produce the large current density H^- beam. We directly study the relation between the extracted beam and the plasma in the arc chamber after cesium injection by experimental method, as shown in the section 4-2 and 4-3.

3. Experimental set-up

3-1. The arc chamber

Figure 3-1 shows a schematic diagram of the ion source. The arc chamber (plasma generator) is 35 cm x 35 cm in cross-section and 18 cm in height. Six tungsten filaments of 1.5 mm in diameter are installed from the side walls of the chamber. The line cusp magnetic field consists of Sm-Co magnets which surround the arc chamber. The external

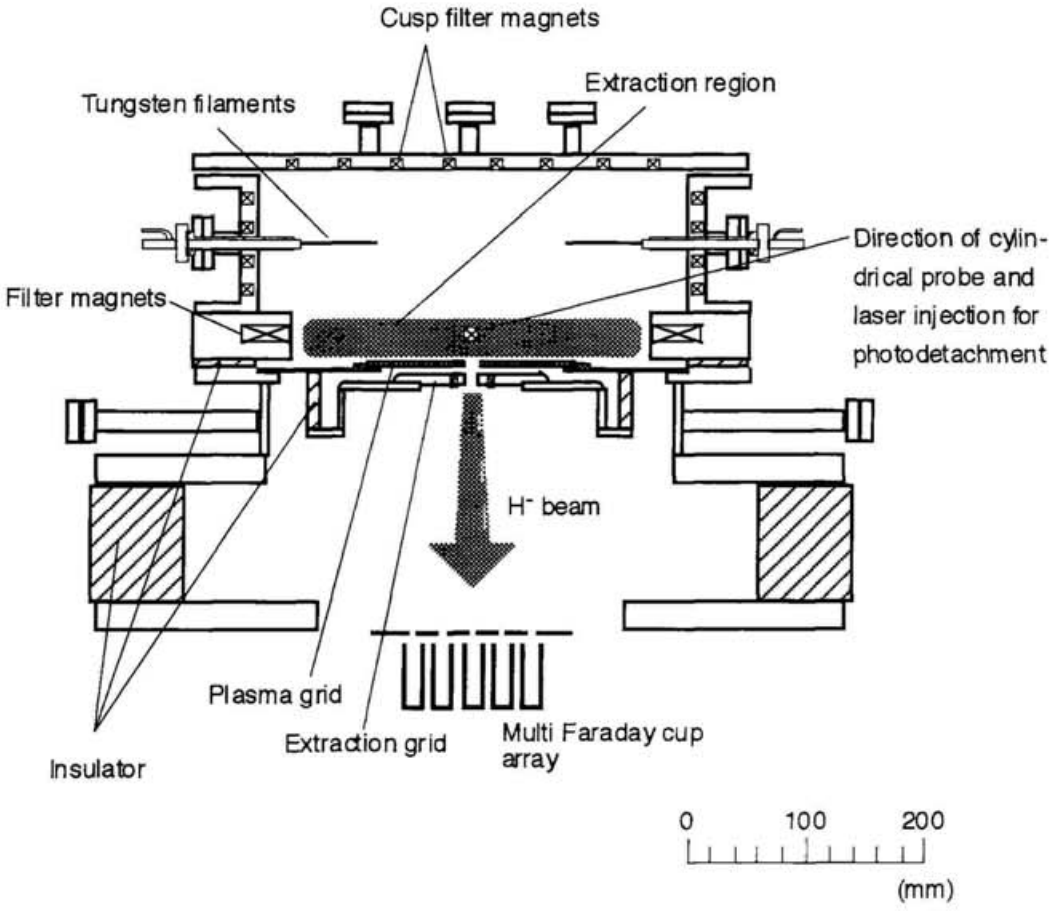

Fig. 3-1. A schematic diagram of the ion source.

filter is adopted for the magnetic separation[14]. The external filter has the advantage in that any structure are not necessary in the arc chamber. This advantage is useful for the H^- measurement by the laser photodetachment method. The dipole magnetic field is produced by a pair of Nd-Fe magnets equipped in front of the plasma grid in the arc chamber, and the field separates extraction region from a high temperature bulk plasma.

Arc discharge is generated in pulse operation for the duration of 500 ms after the filament current stays constant. Repetition periods of each arc discharges are varied from 90 s to 180 s to control the plasma grid temperature which is heated by the radiation from the filament and by the arc plasma.

3-2. Extractor design

The extraction system consists of two grids with one aperture, as shown in Fig. 3-2. A molybdenum plasma grid has a 45° tapered aperture of 5.0 mm in diameter. A copper extraction grid has 9.0 mm aperture in diameter. Two lines of permanent magnets are installed in the extraction grid to deflect the electrons included in the negative ion beam. The thicknesses of the plasma grid and the extraction grid are 2.0 mm and 10.0 mm, respectively. The distance between two grids is set on 3.0 mm. Extraction voltage is varied from 4 kV to 6 kV and H^- current is measured at the voltage at which the beam profile is optimum, i. e. dispersion of the beam profile is smallest.

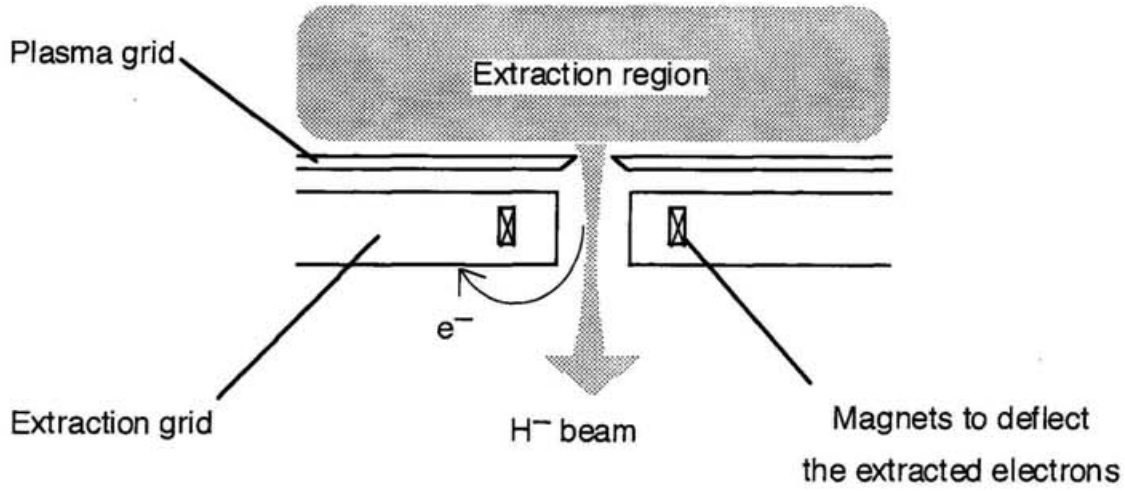

Fig. 3-2. A schematic diagram of the extractor.

3-3. Measurement methods and tools

3-3-1. H^- density measurement using the photodetachment method

The photodetachment method is used for the measurement of the negative ion density[29]. When a laser light is irradiated on the negative hydrogen ion, the ion detaches an electron if the photon energy is larger than the electron affinity of the hydrogen atom E_a (larger than 0.754 eV in energy, or less than 1654 nm in wavelength)

$$H^- + h\nu \ (> E_a) \rightarrow H^0 + e \qquad (3\text{-}1)$$

Here , h is Planck's constant and ν is frequency . A probe immersed in the plasma

containing H^- collects this detached electron if the photodetachment occurs. Detached electron current is observed as the increase of the electron saturation current on the probe biased positively to the plasma. If there is little difference between the electron temperature and the H^- temperature, ratio of the photodetached H^- density ; ΔN_{H^-} to the electron density N_e can be equal to the ratio of the photodetachment signal ΔI^- to the electron saturation current I_{es};

$$\frac{\Delta N_{H^-}}{N_e} = \frac{\Delta I^-}{I_{es}} \tag{3-2}$$

Thus, ΔN_{H^-} can calculate from ΔI^-, I_{es} and N_e.

Figure 3-3 shows the system for the H^- density measurement by the photodetachment method. In this system, a pulse operated Nd-YAG laser (wavelength of 1064 nm)

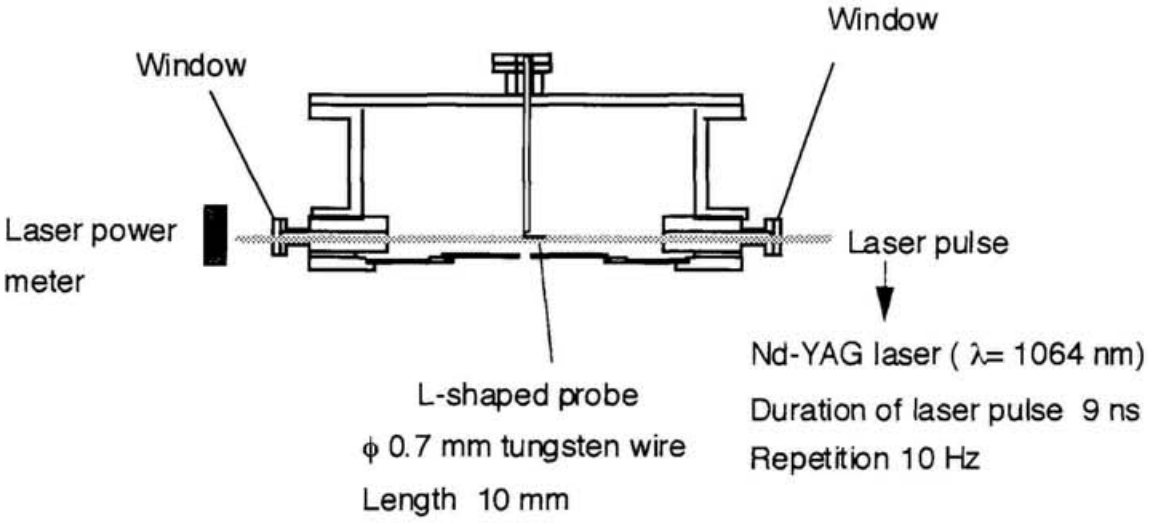

Fig. 3-3. A schematic diagram of the laser photodetachment measurement system.

for 9 ns duration is introduced from the window on the side wall of the arc chamber to pass through the extraction region 15 mm apart from the plasma grid. A cylindrical tungsten probe is located on the laser axis and biased to +40 V with respect to the arc chamber in order to collect the photodetached electrons. To reduce the effect of magnetic field on the probe measurement, the axes of the laser beam and the probe are perpendicular to the line of the magnetic force.

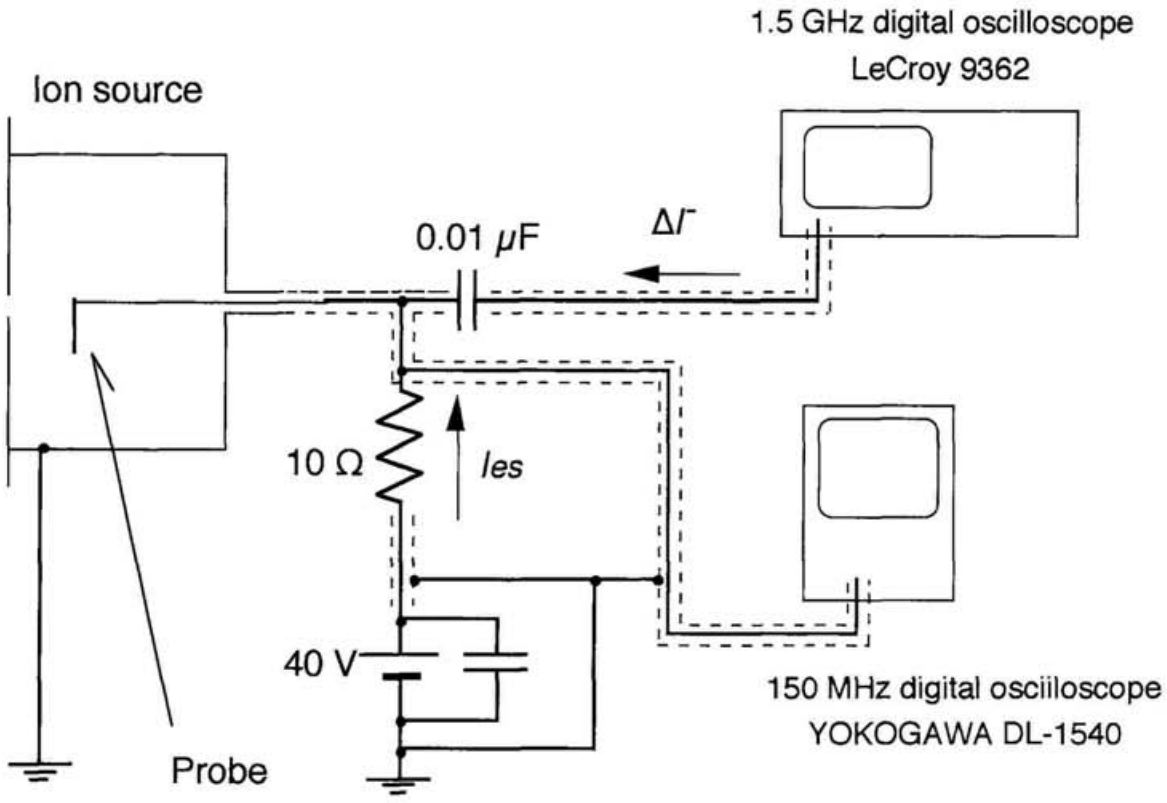

Fig. 3-4. A schematic diagram of the circuit for the photodetachment measurement.

Time scale of a variation of probe signal after a photodetachment is so short that an oscilloscope with the high time resolution is necessary to measure the photodetachment signal. The fast signal of the photodetachment signal ΔI^- is recorded by digital oscilloscope with 1.5 GHz resolution (LeCroy 9362) after it is separated by a capacitance from the constant bias voltage and the slow signal of the electron saturation current I_{es}, which is recorded by another digital oscilloscope with 150 MHz (YOKOGAWA DL-1540), as shown in Fig. 3-4

Figure 3-5 shows an example of the photodetachment signal. Note that the duration of the signal is much longer than the duration of the laser pulse of about 9 ns. The number of the detached H^- by the laser depend on the laser power density. The rate of the photodetached H^-, ΔN_{H^-}, to the H^- in the plasma, N_{H^-}, can be written as follows[29];

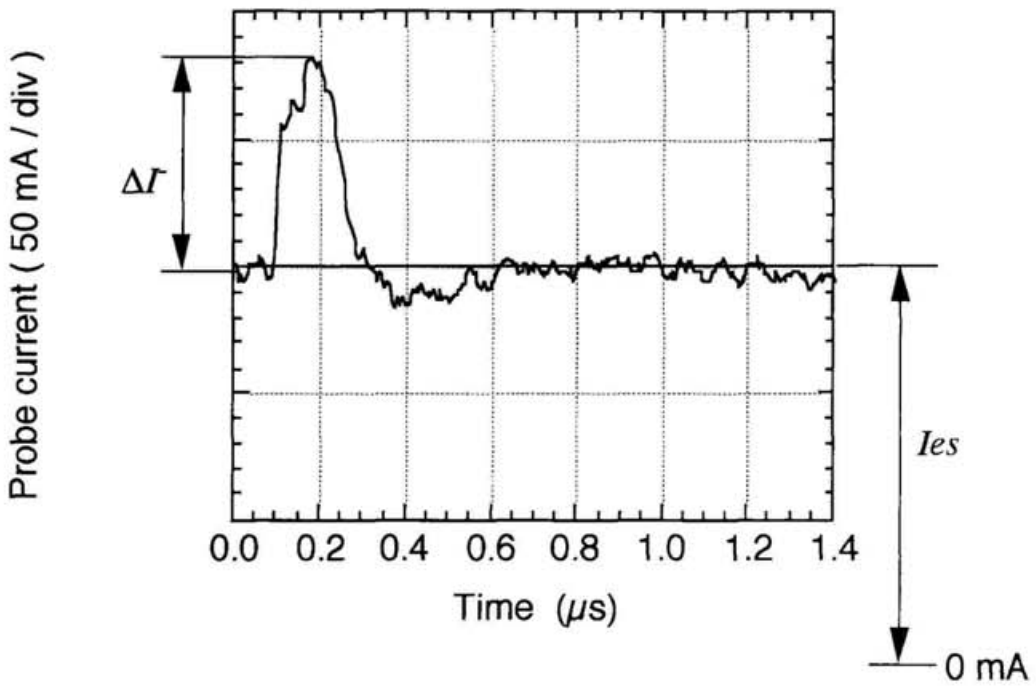

Fig. 3-5. An example of the photodetachment signal.

$$\frac{\Delta N_{H^-}}{N_{H^-}} = 1 - \exp\left(-\frac{\text{Laser pulse energy}}{\text{Laser beam area}} \times \frac{\sigma}{h\nu}\right) \qquad (3\text{-}3)$$

Here, σ; the cross-section of the photodetachment of the H^- by the 1064 nm photon is about 3.6×10^{-17} cm^2 [30]. Then the laser power dependence is calculated as the line of Fig. 3-6. In this figure the dependence of the observed photodetachment ratio on the laser energy density is also shown.

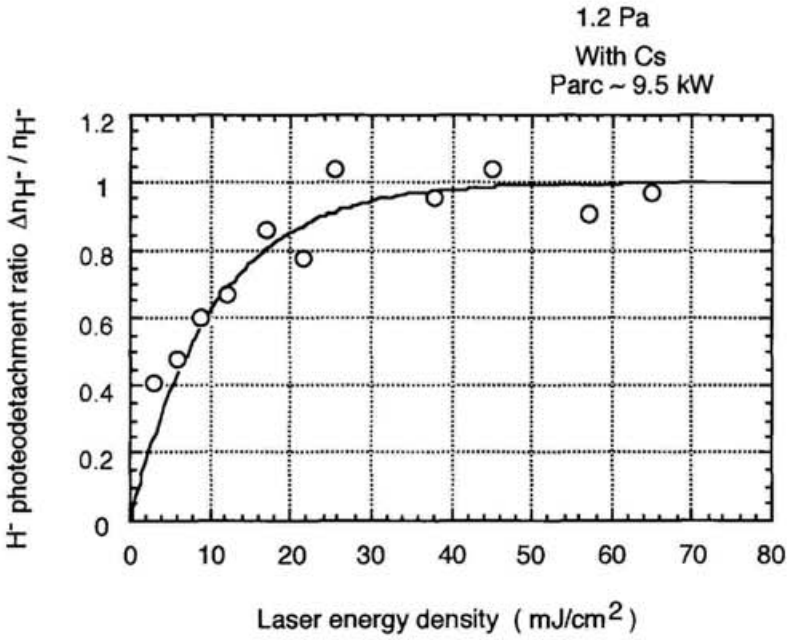

Fig. 3-6. Laser power dependence of the photodetachment ratio to the original H^- ions (here, the electron density and the H^- density in the extraction region are 3.9×10^{11} cm^{-3} and 3.0×10^{11} cm^{-3}, respectively).

The accuracy of the laser power dependence is assured by the data in the cases without and with cesium injection into the arc chamber. According to this data, the laser pulse energy density is fixed at 60 mJ / cm^2 / pulse to detach all H^- ions into H^0 atoms and electrons inside the laser path.

The diameter of a laser beamlet is limited to 6 mm by a collimator, which is enough to reduce the effect of the diameter of probe (0.7 mm) on the photodetachment signal. The collimator diameter is decided by changing the diameter till the saturation of the maximum value of the photodetachment signal is obtained (Fig. 3-7).

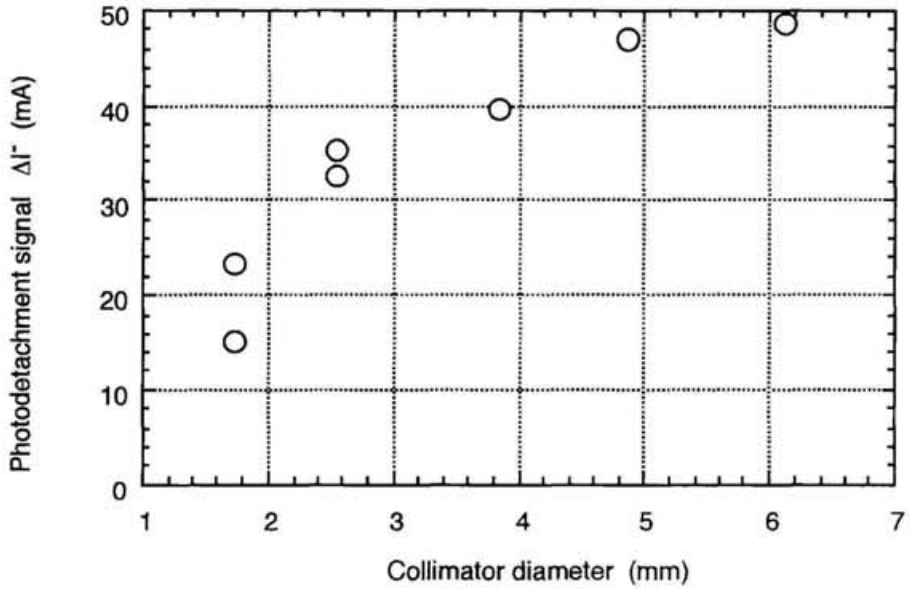

Fig. 3-7. Laser diameter dependence of the photodetachment signal under the constant laser power density (in operating without cesium, pressure 1.5 Pa, arc power 5 kW).

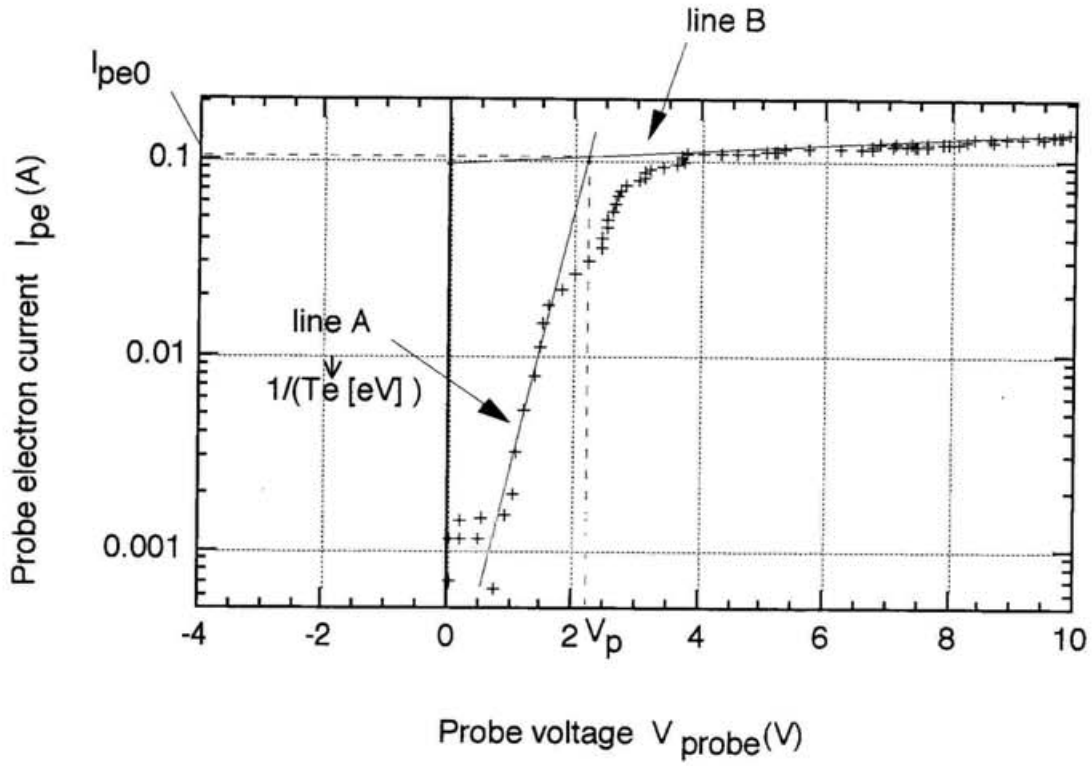

Fig. 3-8. An example of probe trace in the extraction region (in operating with cesium, pressure 1.2 Pa, arc power 12.4 kW).

The other plasma characteristics, such as electron density, electron temperature, are measured by the same single Langmuir probe. Figure 3-8 shows an example of probe signal to measure electron density and temperature.

The probe voltage; V_{probe} is scanned from positive to negative within 0.2 ms ~ 1 ms during an arc discharge. Electron temperature; T_e [eV], electron density; Ne and plasma potential; V_p are calculated as the electron current flowing into the probe; I_{pe}. T_e is calculated as the inverse of the gradient of the line (line A) which is approximately drawn on the retarding potential region of V_{probe} - ln (I_{pe}) plot. V_p is the voltage of the intersection

of line A and the approximation line of electron saturation region (line B). When the surface of the probe is S, Ne is calculate from the current at V_p; I_{pe0}, as follows;

$$N_e\ [\mathrm{cm^{-3}}] = \frac{I_{pe0}\ [\mathrm{A}]}{S\ [\mathrm{cm^2}]\ (T_e\ [\mathrm{eV}])^{1/2}} \tag{3-4}$$

3-3-2. H^- beam current measurement by Faraday cup array

Total ion beam current and its profile are measured simultaneously by the multi-channel Faraday cup array placed at about 20 cm downstream from the exit of the extraction grid. Figure 3-9 shows a schematic diagram of the Faraday cup array. One channel of the Faraday cup consists three parts of oxygen-free-copper. Oxygen-free-copper is used to reduce the gas release from the surface by the collision with the high energy beam ion. The one part is the deep Faraday cup itself; it is 6.0 mm in inner diameter and 14.0 mm in depth, and it has the tapered bottom to reduce the reflection of the captured ions and secondary electrons to the opening of the cup. In front of the cup, there are the reflection plate and the earthed collimator plate. The diameter of the opening on the collimator is 4.0 mm. In order to deflect the electron from the beam plasma in front of the collimator, the reflection plate is biased -15 V to the collimator. The reflection bias works as the reflection force to the secondary electrons in the Faraday cup.

This array is able to remove in the vertical direction. The array consists of 3 channel

vertical array and of 7 channel horizontal array. The vertical array is used to search the center position of the beam. After the array is properly set on the center position of the beam in the vertical position, horizontal beam distribution is measured by the horizontal array. The ion beam density profile $J(x)$ can usually be approximated as a Gaussian profile.

$$J(x) = A \exp \{ - (x-x_0)^2 / \omega^2 \} \qquad (3\text{-}5)$$

On this expression, A means the amplitude of the profile, x_0 means the center position of the beam and ω means the dispersion of the profile. The signals on this Faraday cup array are also similar to a Gaussian profile (Fig. 3-10). The extractor of the source is axisymmetry so that the ion beam is also assumed axisymmetric. Assuming the axisymmetrical Gaussian beam, the total current of the ion source is calculated as

$$I_{H^-} = \pi A \omega^2 \qquad (3\text{-}6)$$

Faraday cup measurement has the advantage in that it shows time variation of the beam current. All the measurements are done at the period when the H^- beam current is approximately constant in time.

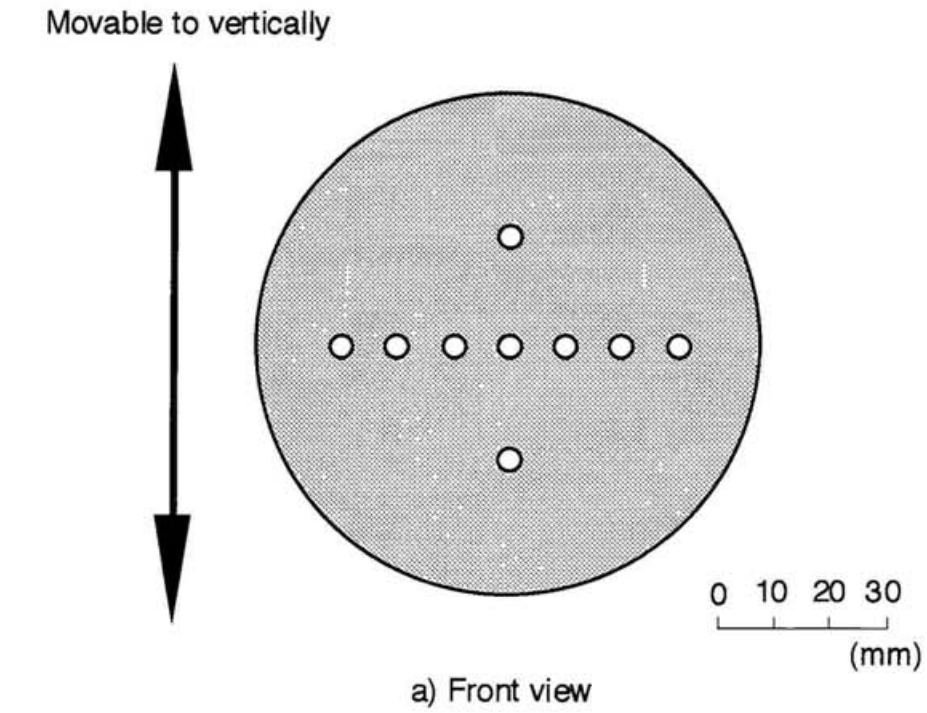

a) Front view

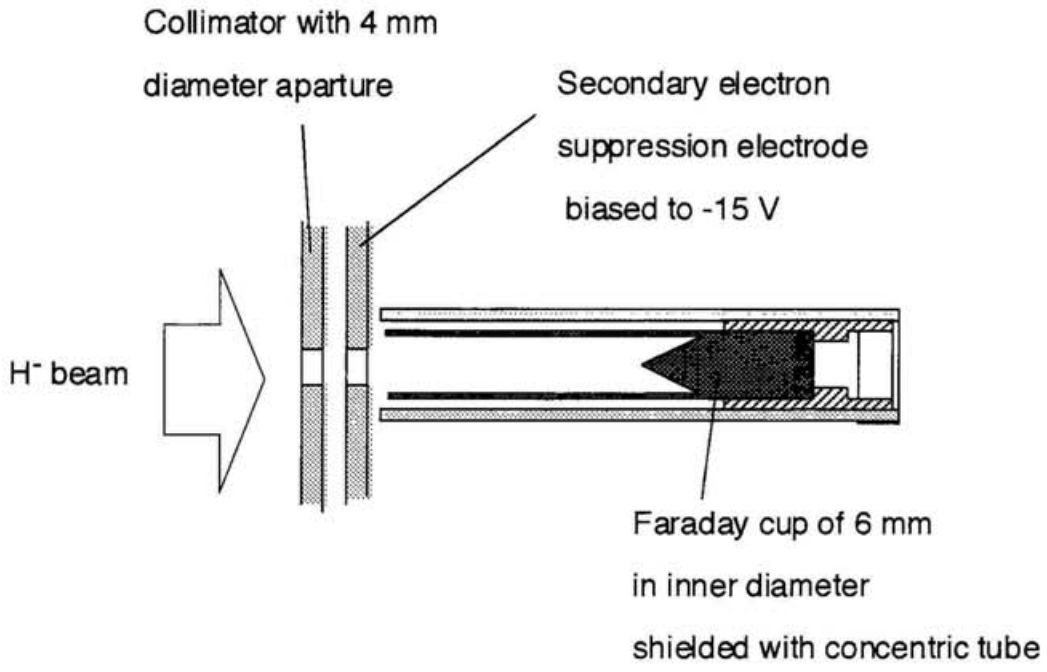

b) Cross-section view

Fig. 3-9. A schematic diagram of the Faraday cup array.

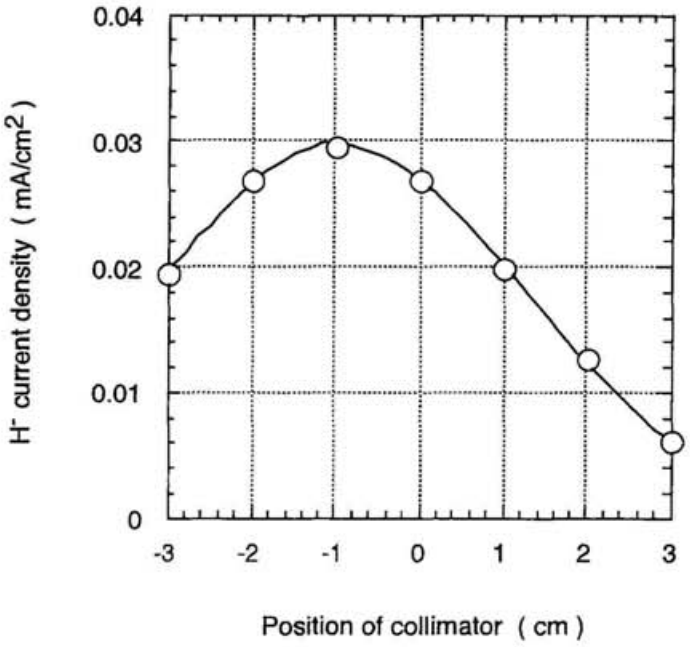

Fig. 3-10. An example of the Faraday cup signal on the horizontal direction. Here, a total H^- current is measured as 0.98 mA at the condition of 1.2 Pa, 10 kW of the arc power, 6.0 kV of the extraction voltage, and operating with cesium.

3-4. Power supplies and their control

Figure 3-11 shows the diagram of the power supply connection on this ion source. Although there is the power supply to add the bias voltage between the plasma grid and the arc chamber, they are directly short-circuited except for the plasma grid bias experiments. Sometimes the enhancement of the H^- beam current at the initial period of the arc discharge is observed and in a short period just after the arc discharge end[31]. In order to observe

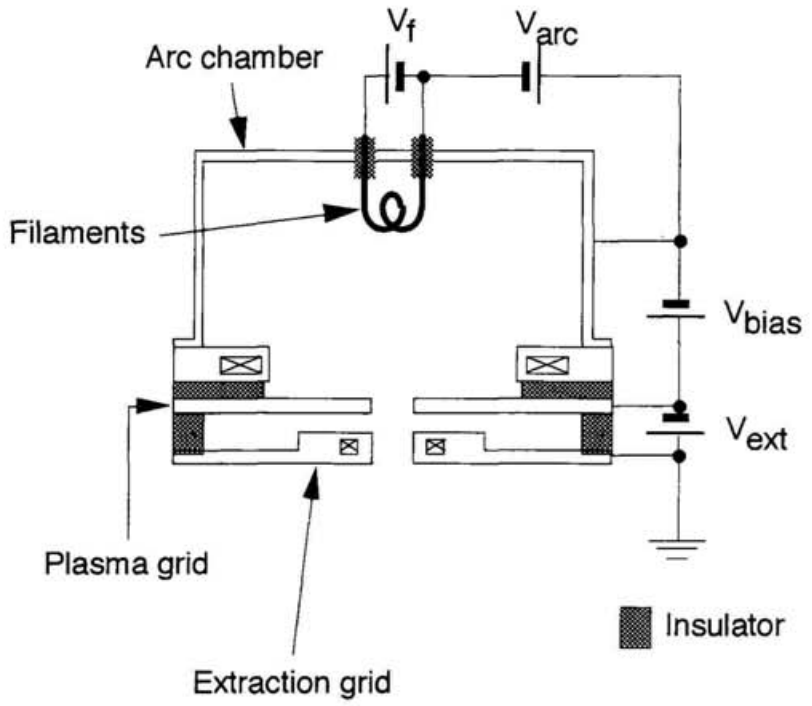

Fig. 3-11. A schematic diagram of the power supply for the ion source.

the time evolution of the measured data, it is very important to synchronize the setting of the time between the ion source operation and the measurement system operation. In our system, the pulse operation of 10 Hz in the Nd-YAG Laser for the photodetachment method is most reliable and not variable, so that this output signal synchronized with Q-switching of the laser power supply is decided as the master clock pulse, as shown in Fig. 3-12. While H_2 gas injection by the piezo-valve and the filament power supply are roughly periodically operated with the main timer unit, the power supply for the arc discharge and the other measurement systems are operated by the combination of the

counter to read the master clock and the delay timers to vary operating periods. Clearance of counting value is done by the signal from the main timer. Figure 3-13 shows the timing diagram of each instruments and typical value. The extraction voltage power supply and the bias voltage power supply is operated constantly in time.

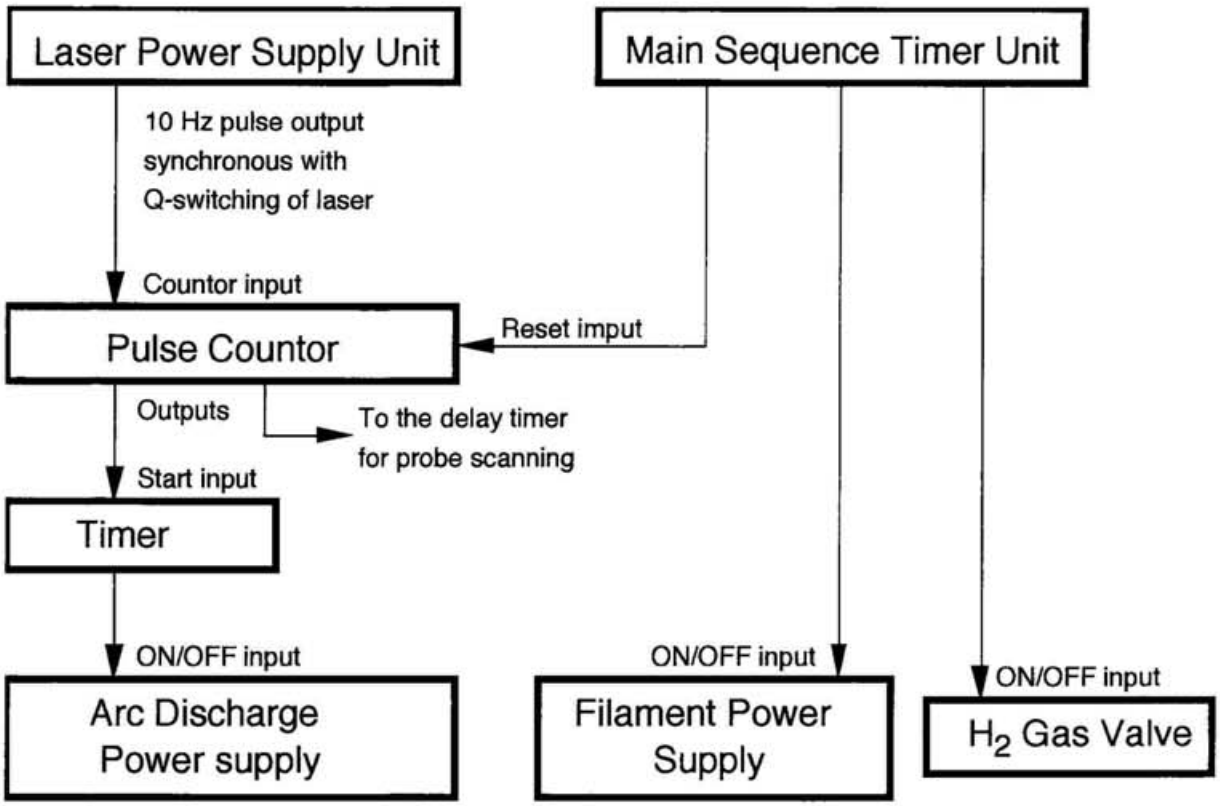

Fig. 3-12. A diagram of timing connection of the operation systems of the ion source.

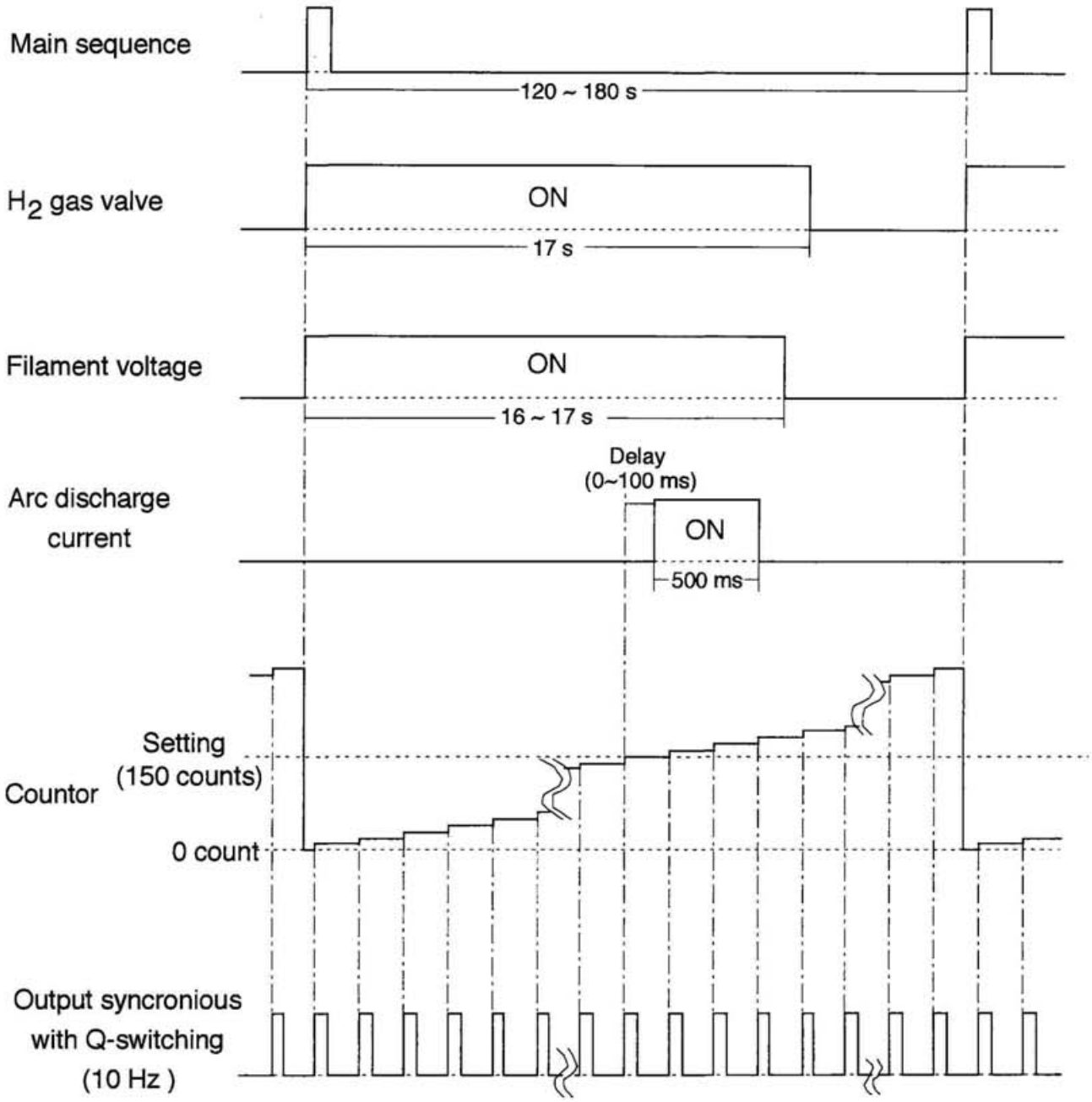

Fig. 3-13. The timing diagram of the operation.

3-5. Gas pumping and injection system

Figure 3-14 shows a schematic diagram of the gas pumping system for the experiment. The pumping system consists of the two lines of pumping unit which has an oil rotary pump and a turbo molecular pump with the pumping speed of 2000 liter / s. Gas injected into the arc chamber from the back plate is pumped not only through the extraction aperture on the plasma grid but also from the four by-pass tube equipped on the side wall of the arc chamber. Gas pressure in the arc chamber is controlled by the voltage supplied to the piezo-valve which is calibrated by the capacitive manometer and monitored by the ionization gauge on the main vacuum chamber.

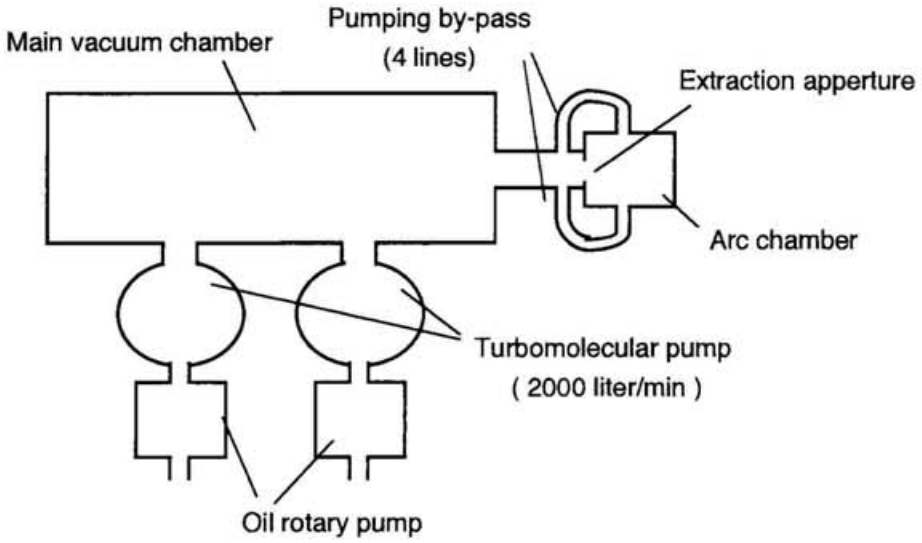

Fig. 3-14. A schematic diagram of the gas pumping system.

4. Experimental results

Here is described the experimental results of the three kinds of the experiments. Detail discussion of the results will appear in the section 5.

4-1. Time evolutions of the plasma characteristics and the extracted beam

A strong time variation of the negative ion density in the ion source was found during the discharge pulse in our ion source at low power discharge with using four spiral-shaped tungsten filaments[32]. At a lower filling gas pressure the negative ion density attained a maximum within 20 ms from the beginning of the discharge and rapidly decreased afterwards. The H^- density reaches its maximum earlier than the electron density (20 ms versus 90 ms), and drops quickly by a factor of four or more. The electron density does not exhibit an important drop after having attained its maximum. At the higher filling pressures there is no maximum in the time evolution of the electron density, which stays almost constant during the pulse. In any cases, time variations of the H^- density does not agree with those of electron density at same condition. This means the production of H^- is effected not only by charged particles in plasma like electrons, but by other neutral particles, as expected from the processes to produce H^-. The difference between a time evolution of the H^- density and that of the electron density in the extraction region is also observed when the six hair-pin-shaped filaments are used (Fig. 4-1).

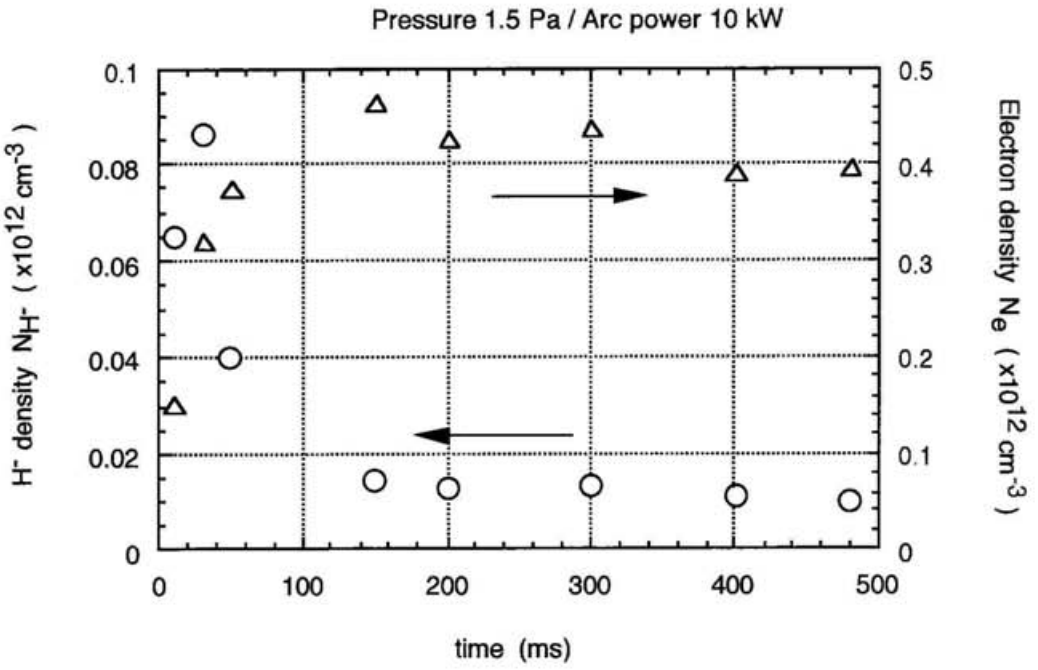

Fig. 4-1. The time evolution of the H^- density (open circle) and the electron density (triangle) in the extraction region at configuration A in operating without cesium.

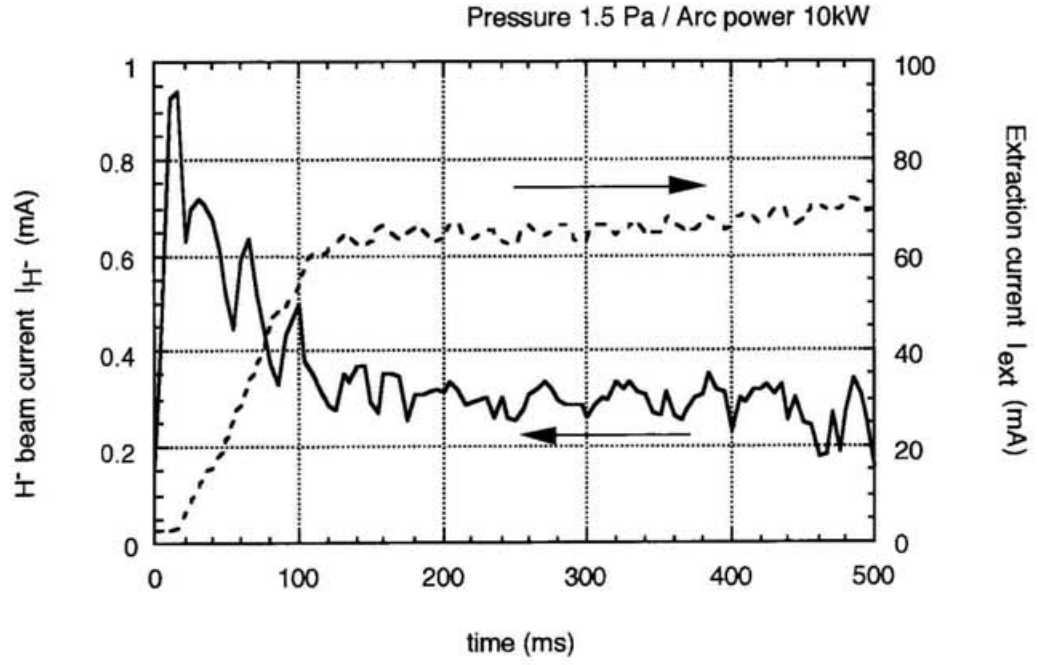

Fig. 4-2. The time evolution of the H^- beam current (solid line) and the electron current (dotted line) extracted from the ion source at configuration A in operating without cesium.

Figure 4-2 shows a time evolution of the H^- beam current and that of electron current extracted from the ion source at the same discharge condition with Fig. 4-1. Figure 4-2 shows obviously that time evolutions of the H^- beam current and the electron extraction current also shows the same variation as those of the H^- density and the electron density in the extraction region.

The existence of this time dependence cannot be observed in the usual tests of the large ion sources for N-NBI, which use time averaged measurements of the particle beam power by calorimetry of the heat load. Since the H^- beam extraction is measured by the Faraday cup array in our system, time evolution of the H^- current is able to observe.

4-2. The effect of the filter magnetic field strength

In this part two kinds of the filter magnetic field are examined and compared on the non- cesium operation. The purpose of this experiment is not only the observation of the effect of the filter field, but also the construction of the database on the non-cesium operation so as to compare with the cesium operation in the next section. In addition, optimization of the filter field is intended by changing the filter field strength.

Figure 4-3 shows the magnetic flux distribution by the magnetic filter on the center axis in the arc chamber. The line density of the magnetic field of the configuration A is 750 G•cm and the one of the configuration B is 1600 G•cm.

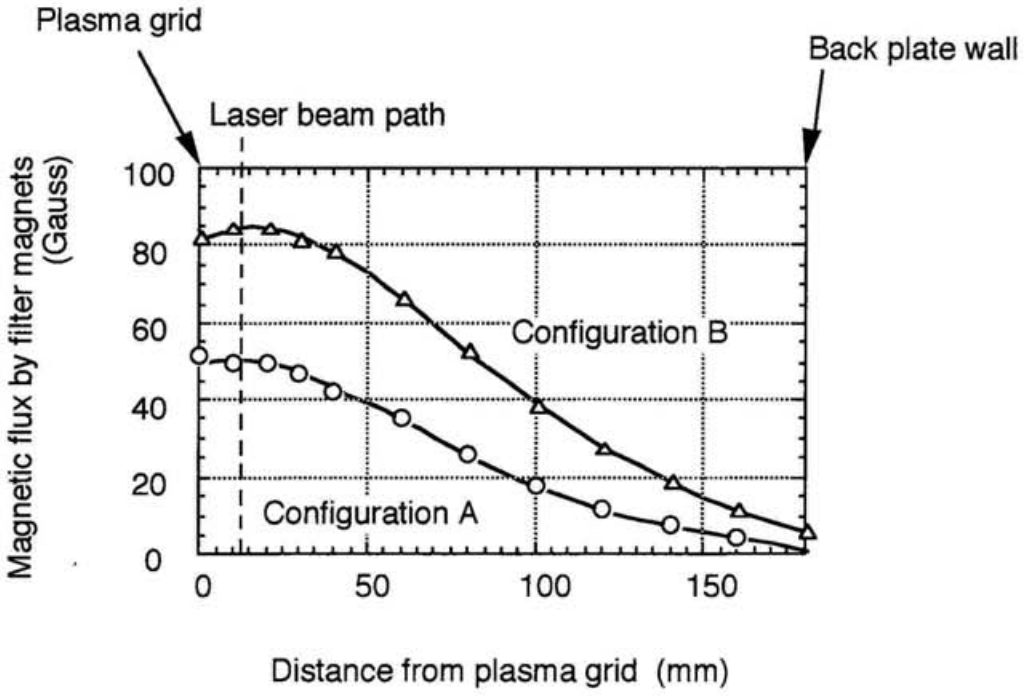

Fig. 4-3. Measured filter magnetic field distribution on the center axis of the ion source. (circle; configuration A: weak magnetic field of 750 G • cm, triangle; configuration B: strong magnetic field of 1600 G • cm)

Figure 4-4 shows the arc power dependence of the H^- beam current extracted from the ion source for configuration A. Variation of extracted electron current according to the arc power at the configuration A is shown in Fig. 4-5. Both of the H^- beam current and the extracted electron current increase at low arc power as the arc power is raised. Then the H^- beam current steeply decreases as the arc power is higher while the electron current increases higher and higher. The decreasing tendency is also observed on the H^- density characteristics, as shown in Fig. 4-6. Electron density in the extraction region simply increase as the arc power increase (Fig. 4-7), as well as extracted electron current.

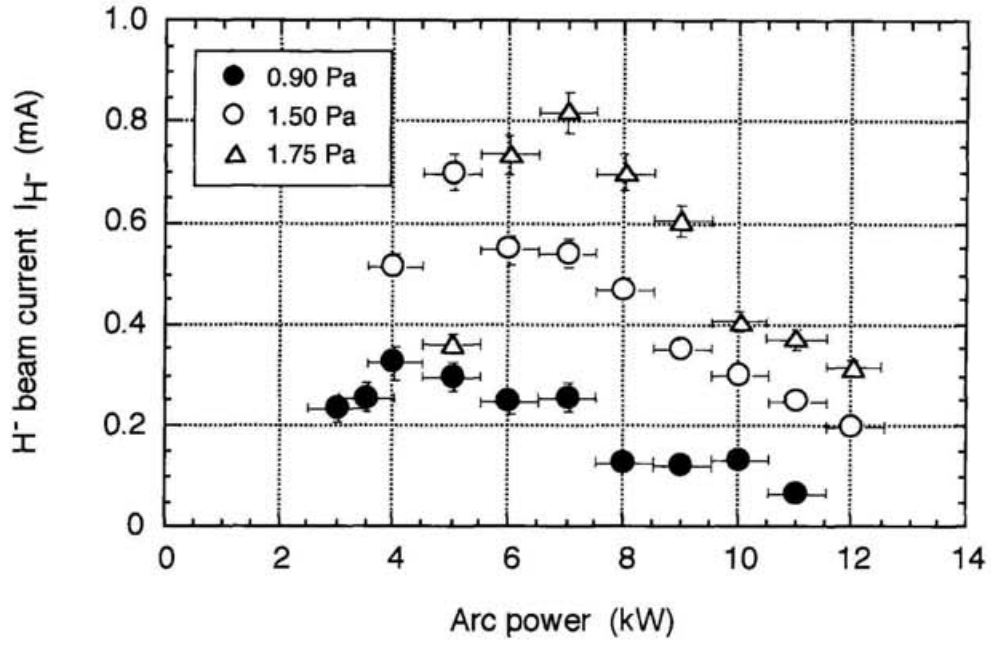

Fig. 4-4. The discharge arc power dependence of the H^- beam current extracted from the ion source at configuration A.

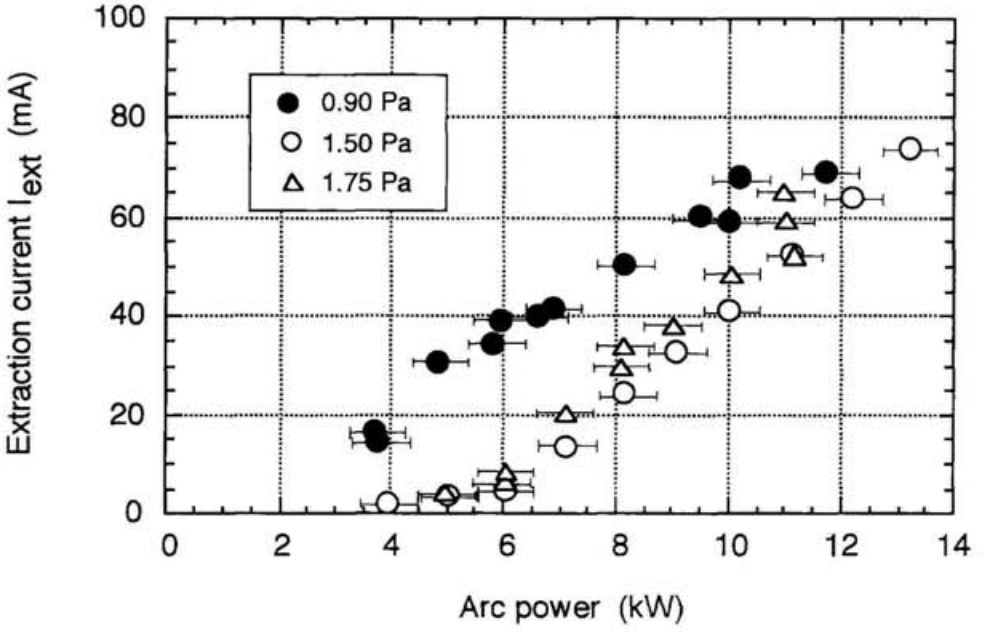

Fig. 4-5. The discharge arc power dependence of the extracted electron current from the ion source at configuration A.

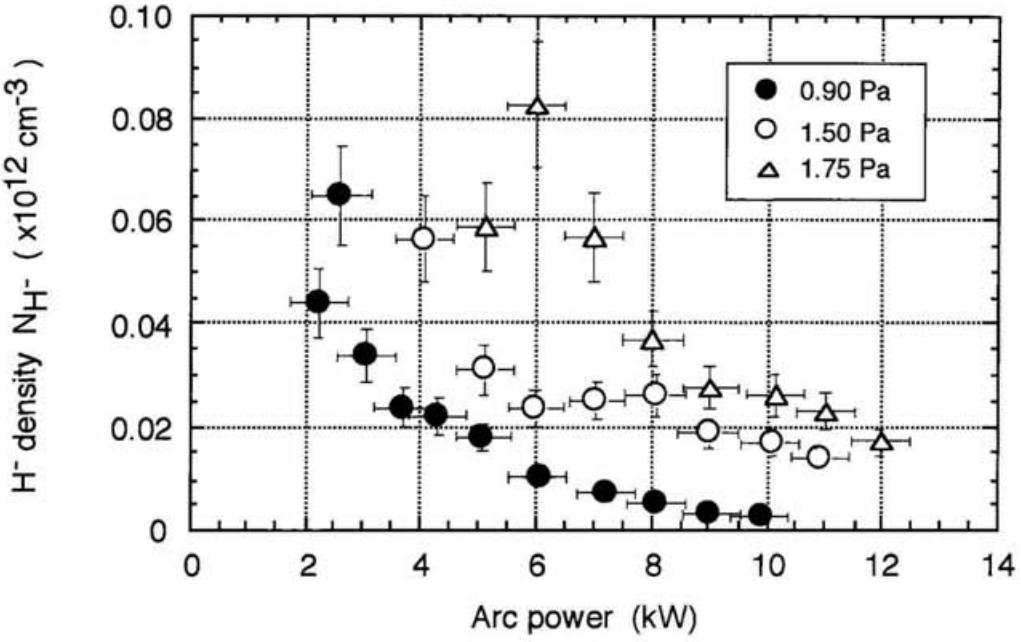

Fig. 4-6. The discharge arc power dependence of the H^- density in the extraction region at configuration A.

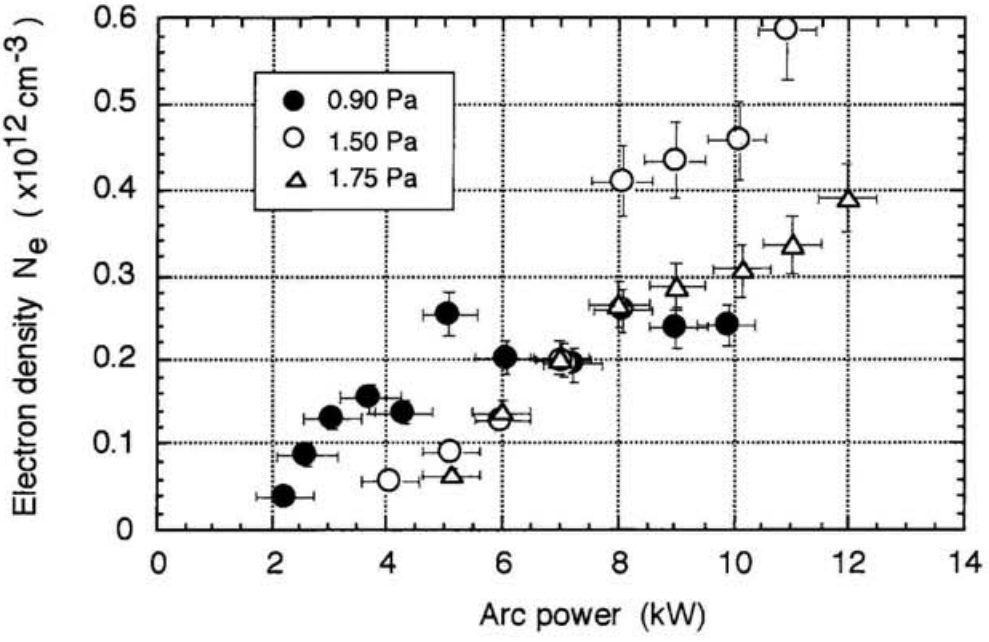

Fig. 4-7. The discharge arc power dependence of the electron density in the extraction region at configuration A.

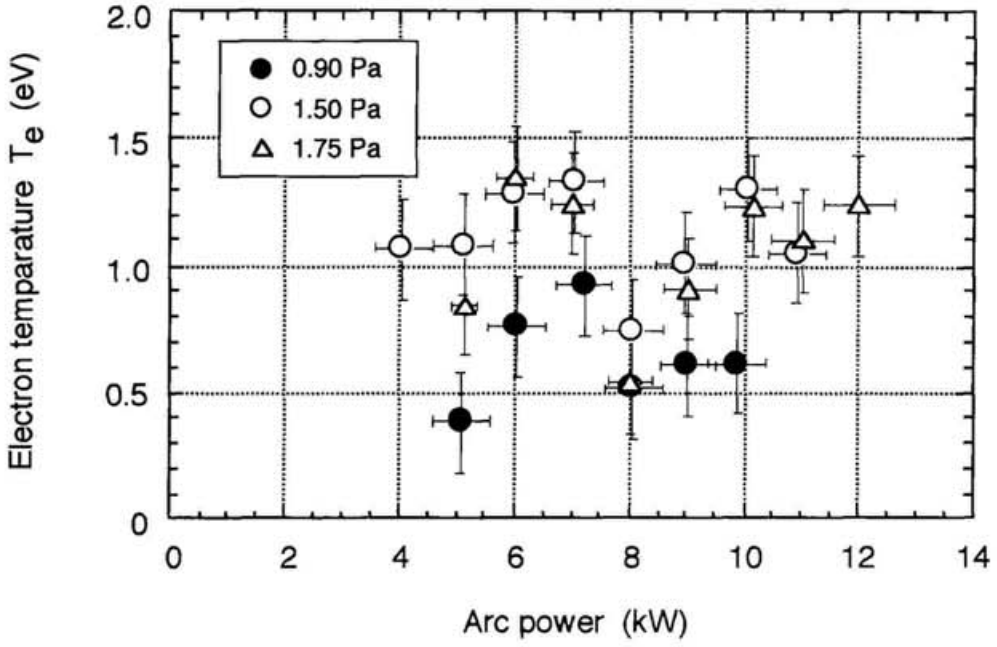

Fig. 4-8. The discharge arc power dependence of the electron temperature in the extraction region at configuration A.

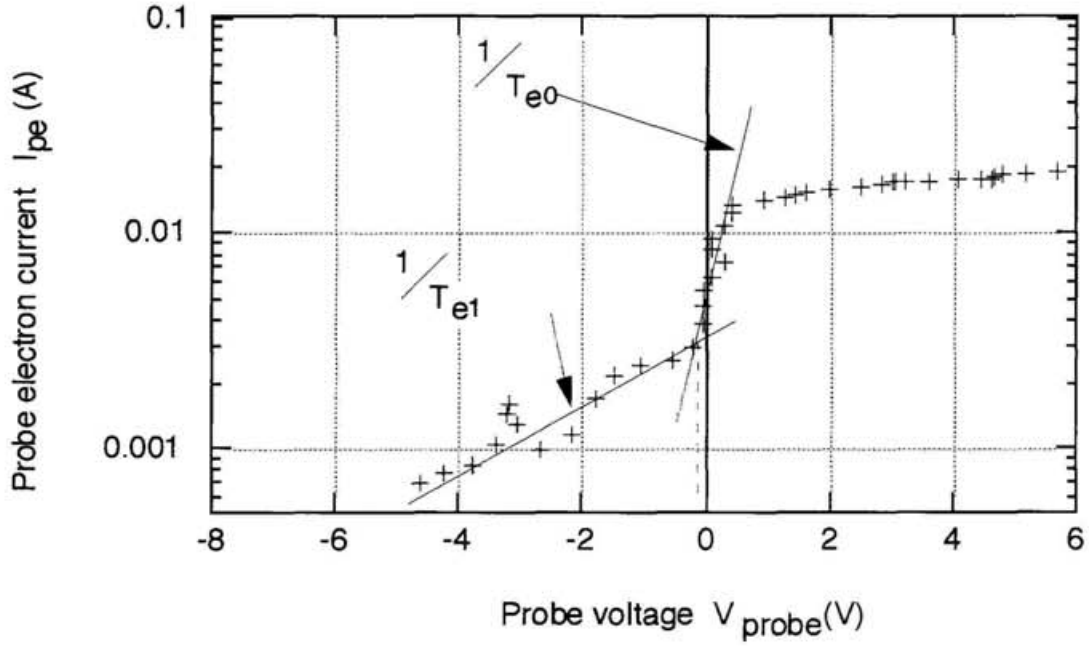

Fig. 4-9. An example of the probe trace at configuration A. It can be seen that there are two components in electron temperature.

At configuration A, electron temperature has little dependence on the arc power as shown in Fig. 4-8, and high energy tail of electron distribution is seen by probe trace. Figure. 4-9 shows an example of the probe trace with high energy tail. Assuming that the distribution function of electron is the sum of two Maxwell distribution, i. e., main part of temperature; T_{e0} (eV) and density; N_{e0}, and high temperature part of T_{e1} (eV) and N_{e1} ($T_{e0} < T_{e1}$), then electron current into the probe can be express as follows;

$$I_e = I_{e0} \exp\left(-\frac{V}{T_{e0}}\right) + I_{e1} \exp\left(-\frac{V}{T_{e1}}\right) \tag{4-1}$$

Here, $I_{e0} = \frac{1}{4} N_{e0} Se \left(\frac{8eT_{e0}}{\pi m}\right)^{1/2}$, $I_{e0} = \frac{1}{4} N_{e0} Se \left(\frac{8eT_{e1}}{\pi m}\right)^{1/2}$

When probe traces at configuration A are analyzed again based on the expression above, temperatures and density ratio can be graphed as Fig. 4-10. From this figure it is obvious that the temperature of main part doesn't vary but that of high temperature part rise up and its density ratio become higher at higher arc power. Hence it is concluded that the more high energy electron penetrate into the extraction region and destruct H^- ions by collision and this lead the decrease of the H^- density at higher arc power. Thus, the configuration A is seemed to be insufficient to produce enough filter field. For the purpose of achieving the stronger suppression of high energy electrons flowing into the extraction region from dense plasma in the driver region, the magnetic filter is exchanged to the configuration B with stronger field.

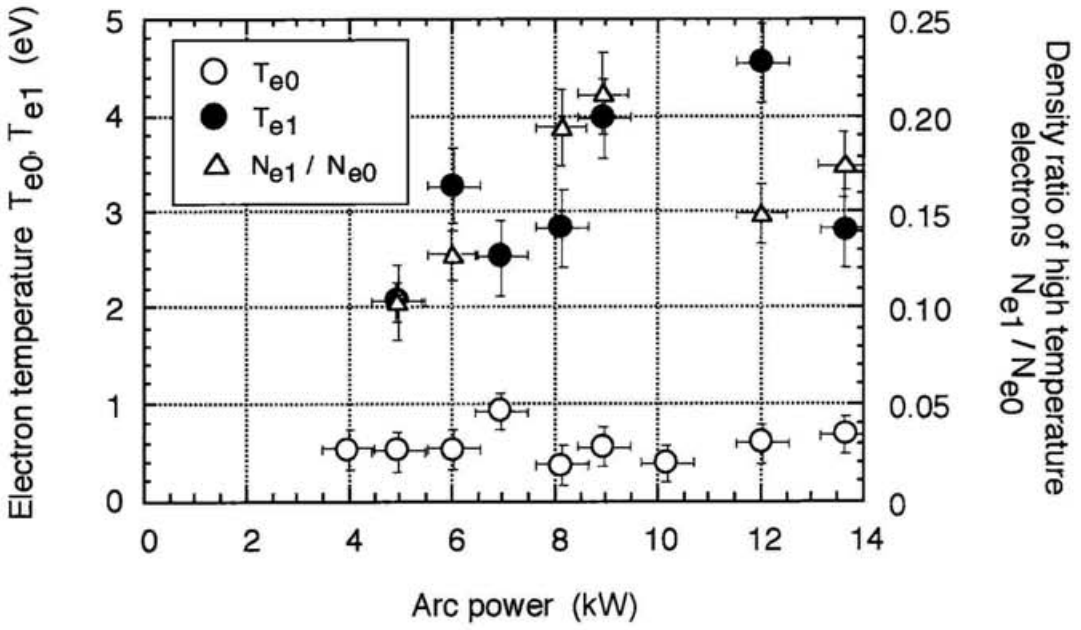

Fig. 4-10. The discharge arc power dependence of the electron temperature T_{e0} (main component), T_{e1} (high temperature component) and the density ratio of the high energy tail to the main electrons in the extraction region at configuration A at gas pressure; 1.2 Pa.

Figures 4-11 and 4-12 shows the arc power dependence of the H^- beam current and extracted electron current from the ion source at the configuration B, respectively. While figures 4-13 and 4-14 shows the arc power dependence of the H^- density and the electron density in the extraction region at the configuration B, respectively. It is obvious in this case that the performance of the ion source is improved, i. e. the numbers of H^- ions are not decreased but saturated at the high arc power. The power at which the H^- density saturates is higher as gas pressure is higher, as well as the configuration A. A maximum H^- density is not so different between the configuration A and B while electron density at the configuration B is lower than that of the configuration A by stronger magnetic field. Hence the density ratio of H^- ions to electrons in the extraction region is much higher at the

configuration B. This is also proved by reduction of the electron current extracted with the H^- beam. The configuration B shows the improvement of property in that H^- ions' ratio to electrons increases. The probe measurements doesn't show high energy tail of electron distribution so that high energy electron is suppressed enough in the extraction region by using stronger magnetic field. Hence electron temperature is decreased by using the stronger filter; the configuration B (Fig. 4-15).

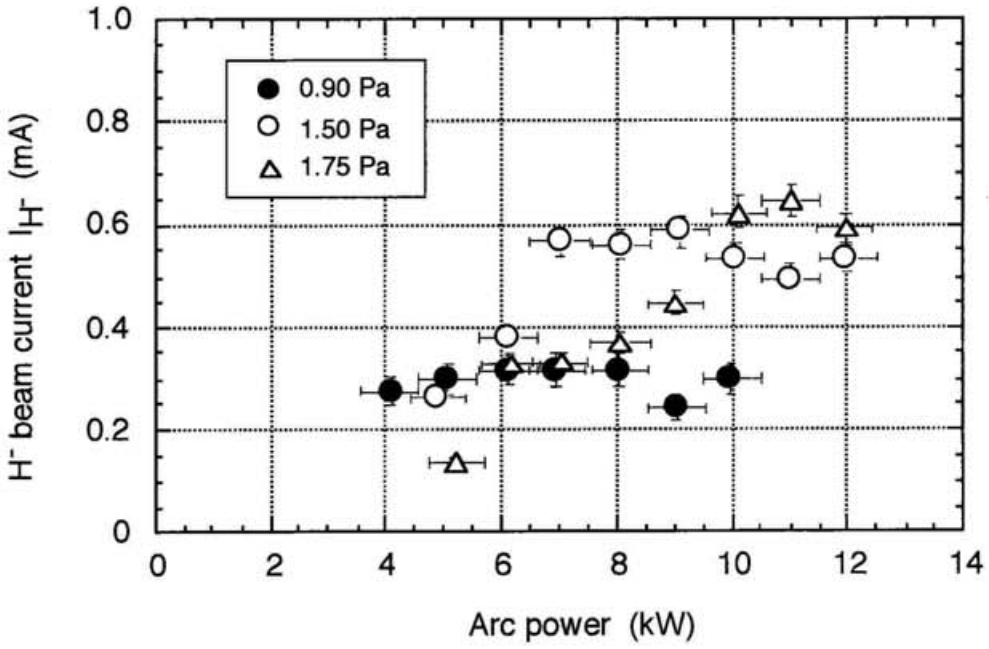

Fig. 4-11. The discharge arc power dependence of the H^- beam current extracted from the ion source at configuration B.

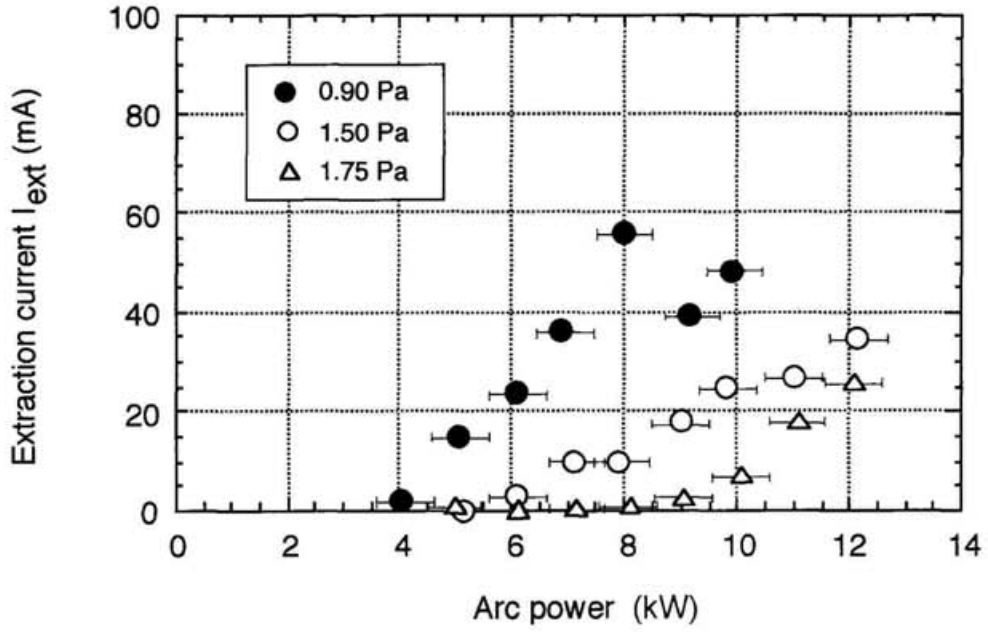

Fig. 4-12. The discharge arc power dependence of the extracted electron current from the ion source at configuration B.

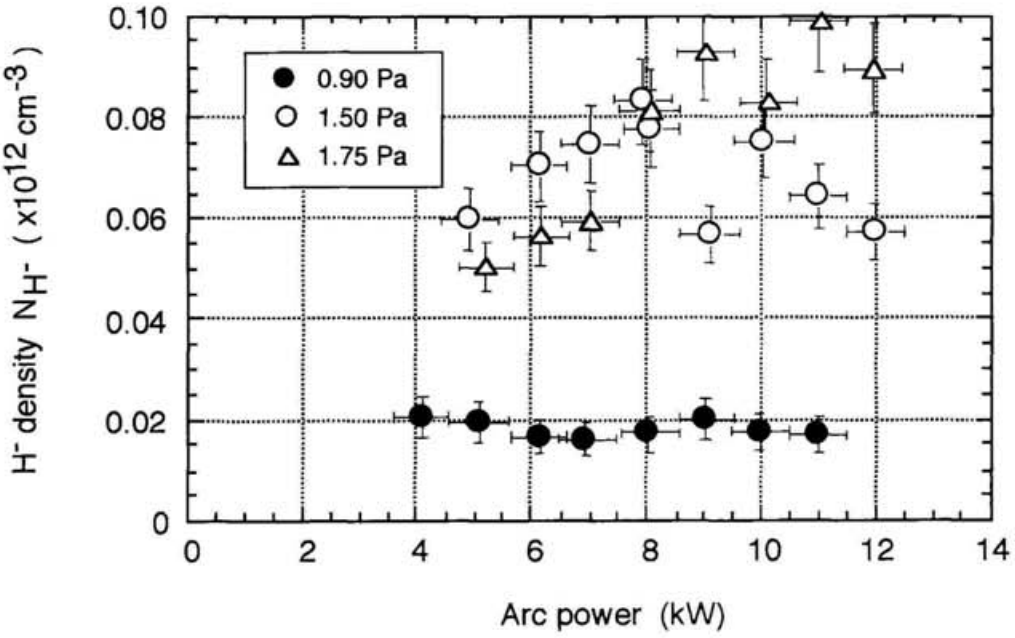

Fig. 4-13. The discharge arc power dependence of the H^- density in the extraction region at configuration B.

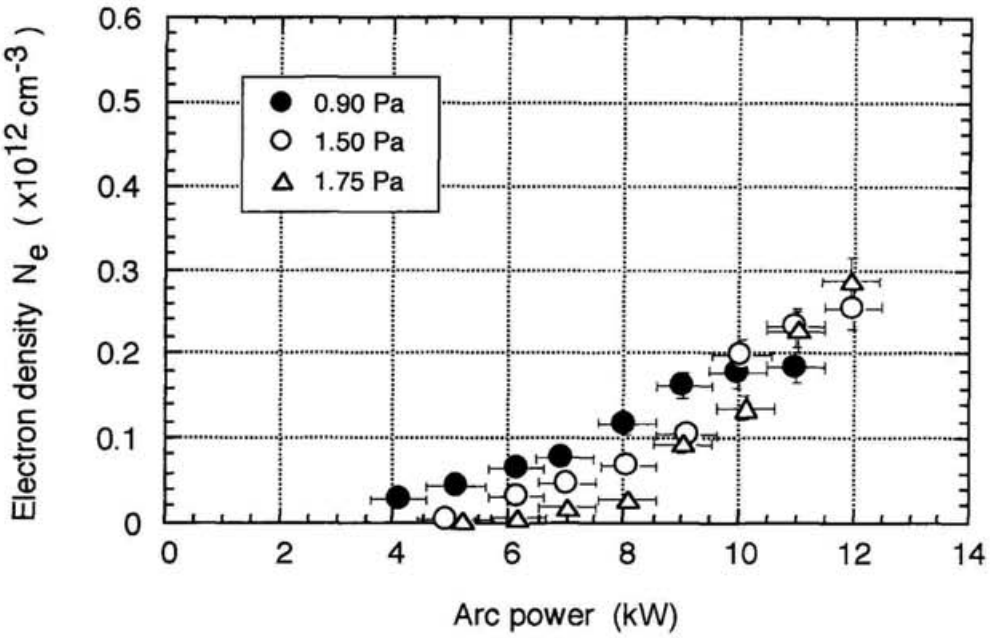

Fig. 4-14. The discharge arc power dependence of the electron density in the extraction region at configuration B.

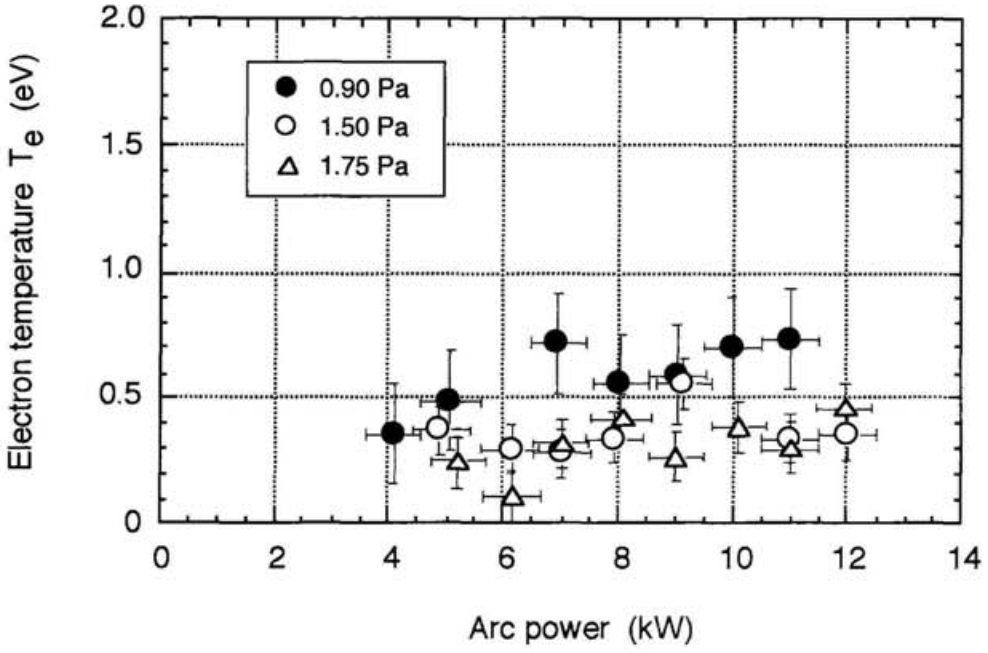

Fig.4-15. The discharge arc power dependence of the electron temperature in the extraction region at configuration B.

4-3. The effect of introduction of cesium vapor into the ion source

In ordinary operation of a volume-production-type H^- source, an extracted H^- beam current increases and an extracted electron current decreases after introducing cesium vapor into the arc chamber[3]-[5][8][9]. These effect of cesium introduction is also recognized in this study. Plasma parameter measurements and H^- density measurements by photodetachment are followed after it is recognized that the cesium effect is enough.

In injecting cesium vapor into the ion source, the contamination of cesium or cesium compound on the probe is a serious problem. In this study, the laser pulse of 60 mJ / cm^2 - 10 Hz is continuously radiated on the probe to avoid the contamination all the time when the ion source is operated with cesium in the arc chamber.

Figures 4-16 and 4-17 show the arc power dependence of the extracted H^- beam and extracted electron current after the cesium effect appeared, respectively. the H^- beam current after the cesium injection increase as twice as the beam current without cesium vapor, whereas the electron current decreases by less than 1/10 of the non-cesium operation. Therefore the cesium effect on the extracted beam is observed also in the ion source of this study.

The H^- density in the extraction region is shown in Fig. 4-18 and the electron density and temperature are shown in Fig. 4-19 and Fig. 4-20, respectively. Obviously the H^- density in the extraction region increases after the cesium injection and its increasing ratio is higher than the ratio of the extracted beam.

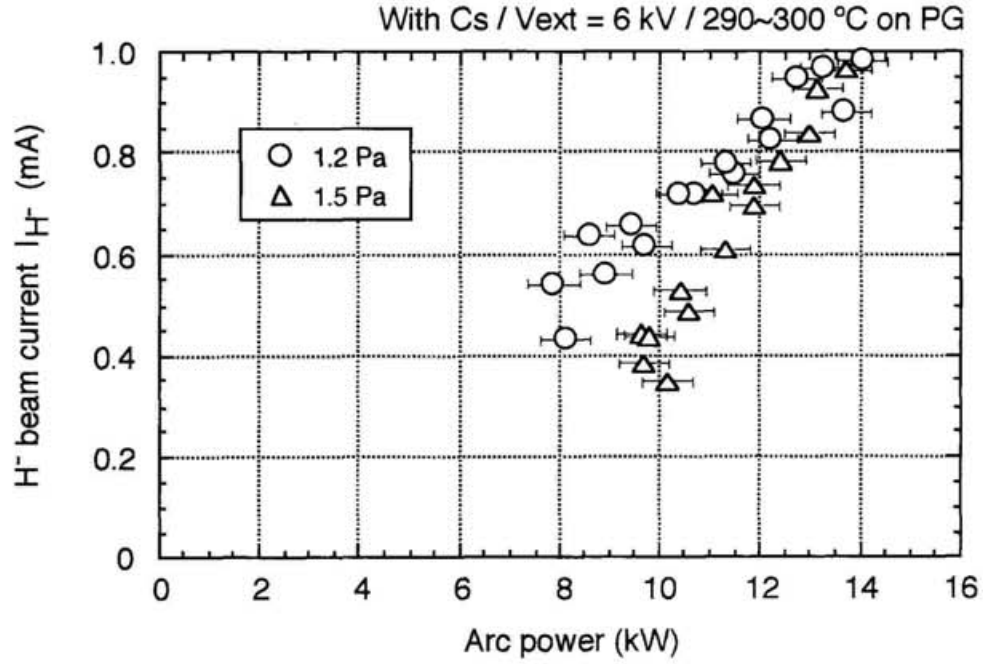

Fig. 4-16. The discharge arc power dependence of the H^- beam current extracted from the ion source with injection of the cesium vapor into the arc chamber.

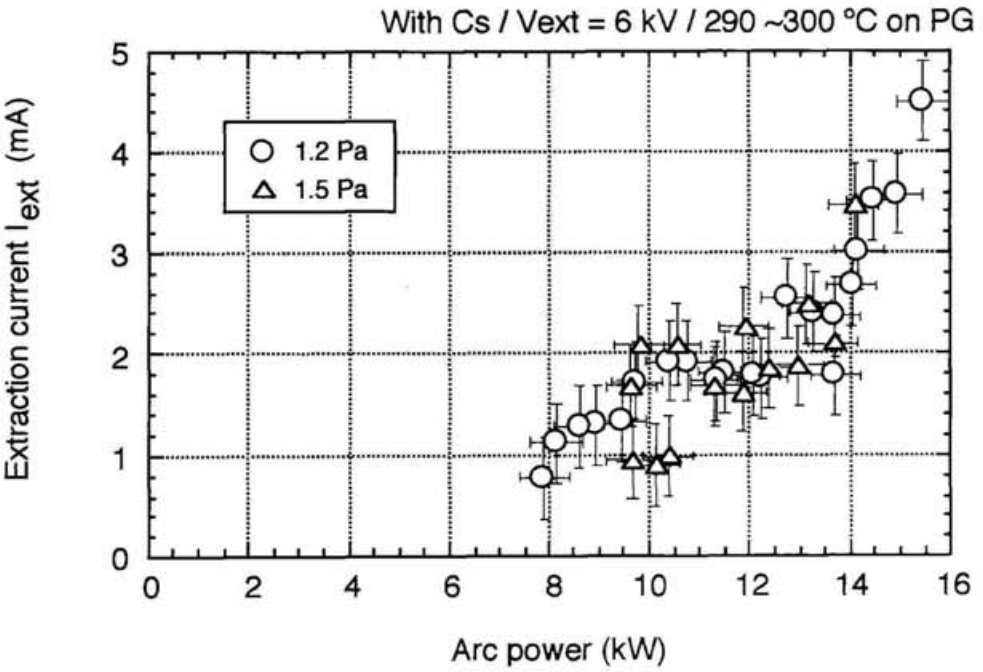

Fig. 4-17. The discharge arc power dependence of the extracted electron current from the ion source with injection of the cesium vapor into the arc chamber.

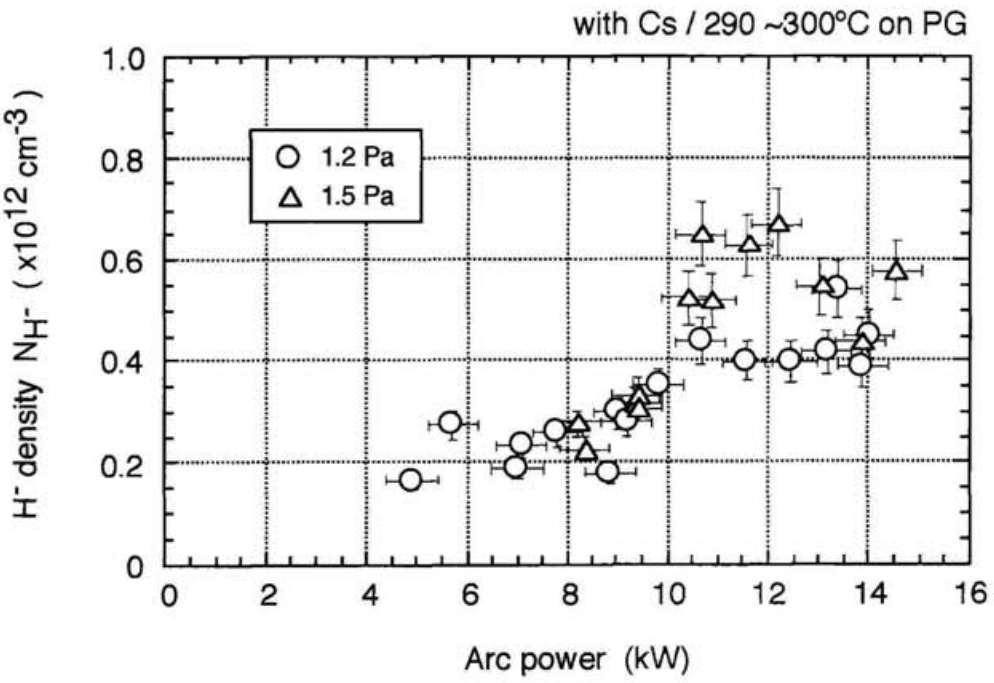

Fig. 4-18. The discharge arc power dependence of the H^- density in the extraction region with injection of the cesium vapor into the arc chamber.

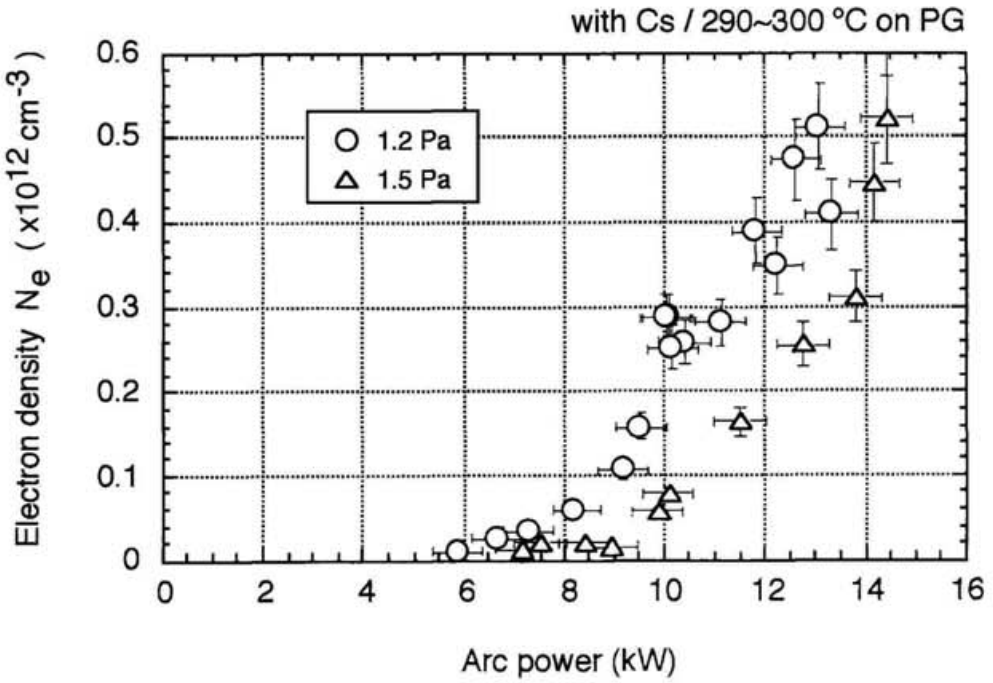

Fig. 4-19. The discharge arc power dependence of the electron density in the extraction region with injection of the cesium vapor into the arc chamber.

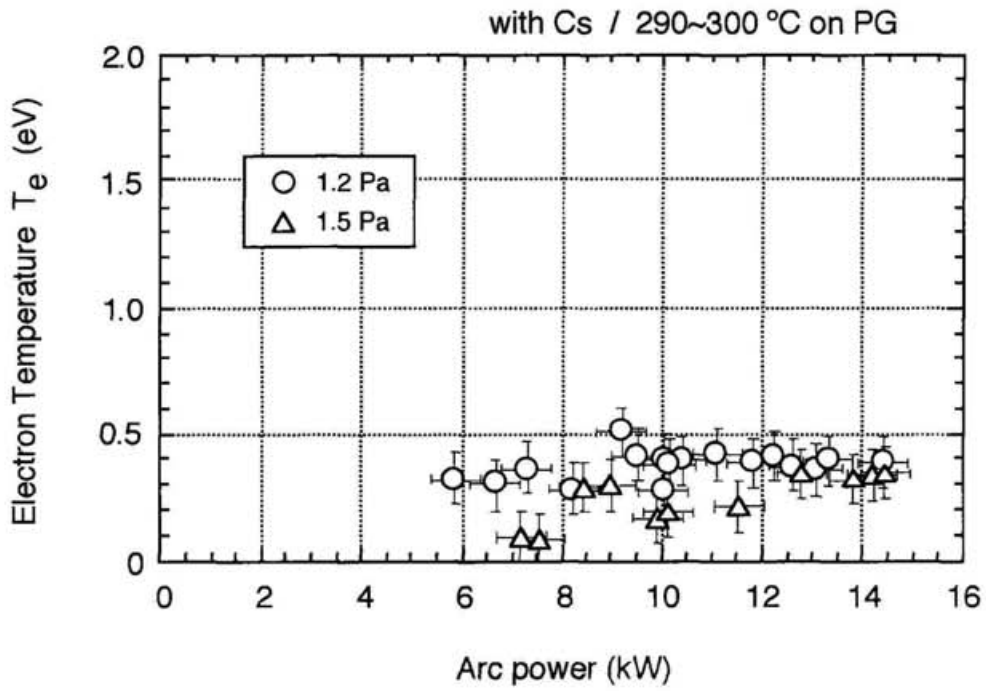

Fig.4-20. The discharge arc power dependence of the electron temperature in the extraction region with injection of the cesium vapor into the arc chamber.

4-4. The effect of addition of the bias voltage

The positive bias voltage is applied on the plasma grid with respect to the arc chamber in order to reduce the electron current involved in the extracted H^- beam[9][13]. Figures 4-21 and 4-22 show the bias voltage dependence of the extracted H^- beam current and the extracted electron current, respectively, in the case of the ion source of this study under the operation with cesium. Similar to other H^- sources, the electron current steeply decreases and the H^- current starts decreasing from some value of the bias voltage, in this

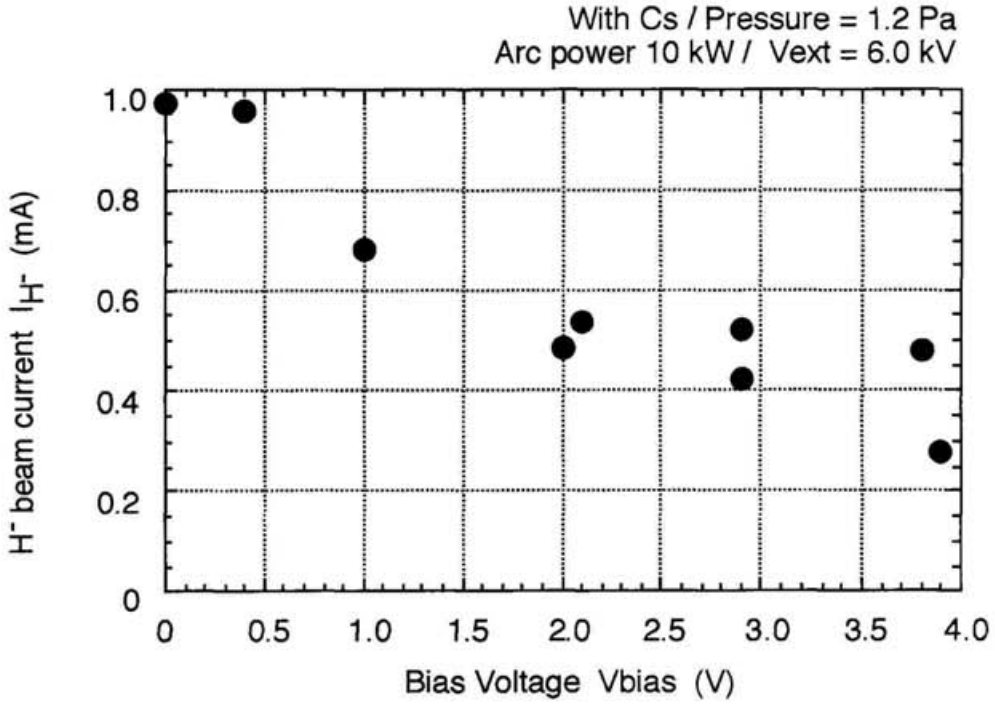

Fig. 4-21. The bias voltage dependence of the H^- beam current extracted from the ion source with injection of the cesium vapor into the arc chamber.

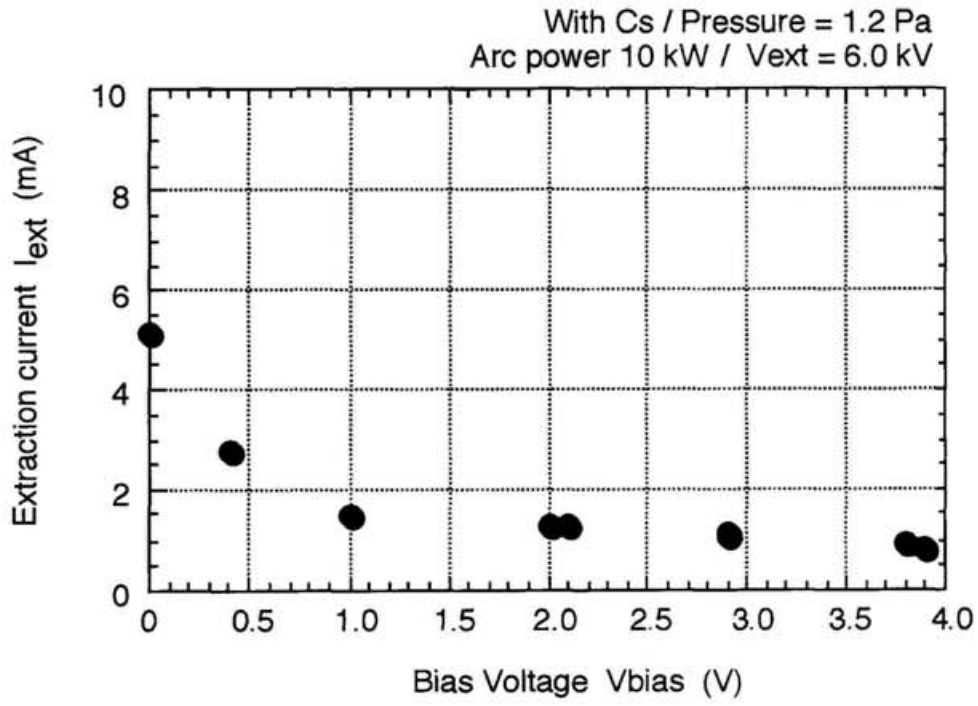

Fig.4-22. The bias voltage dependence of the extracted electron current from the ion source with injection of the cesium vapor into the arc chamber.

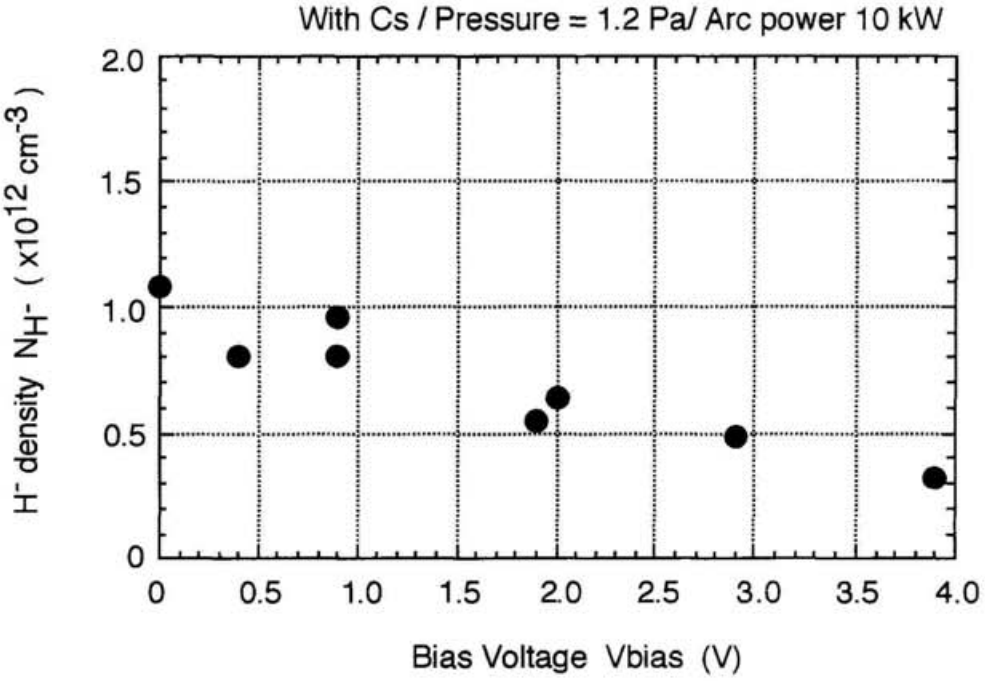

Fig. 4-23. The bias voltage dependence of the H^- density in the extraction region with injection of the cesium vapor into the arc chamber.

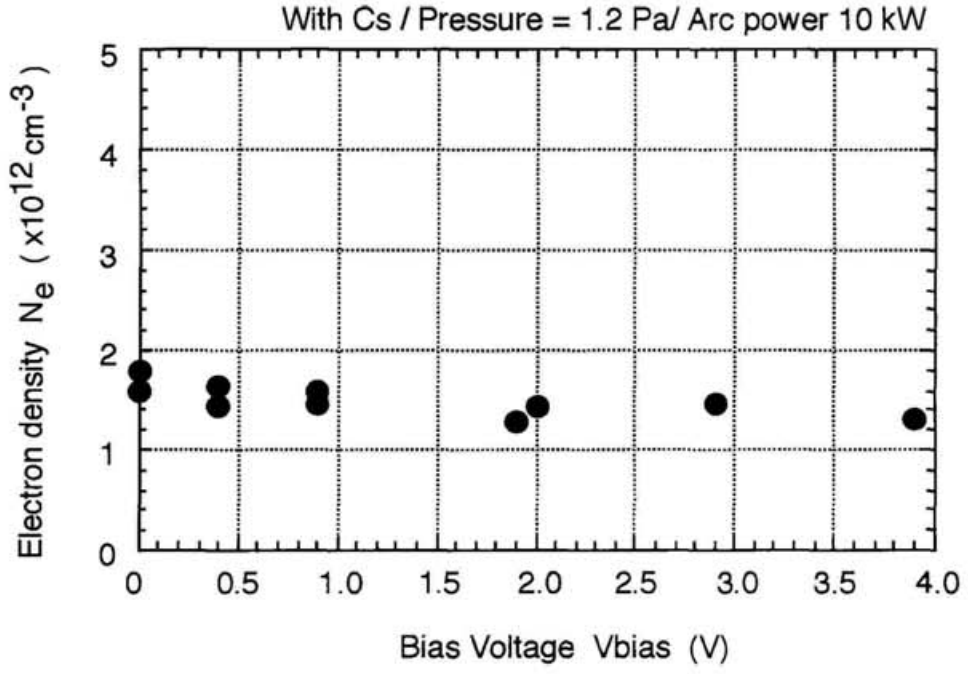

Fig. 4-24. The bias voltage dependence of the electron density in the extraction region with injection of the cesium vapor into the arc chamber.

case 1 V, and the saturated H^- current is not much smaller than maximum value. The H^- density and the electron density in the extraction region are shown on Fig. 4-23 and 4-24, respectively. It can be seen that the electron density is independent of the bias voltage. Comparing the extracted H^- and the electron currents, the tendencies of the H^- beam and the H^- density are not so different with bias voltage, but behaviors of the electrons in the plasma and those extracted are different.

5. Discussion

5-1. The relation between the extracted H^- beam current and the H^- density in the extraction region

It is observed from Fig. 4-4, 4-6 and Fig. 4-11, 4-13 that the H^- density in the extraction region and the extracted H^- beam current obviously have correlation in the volume-production-type H^- source. The relationship of the H^- beam current with the H^- density is shown on Fig. 5-1. Naturally, it is necessary to effectively produce H^- ions in the extraction region in order to extract a H^- beam efficiently. Although dense plasma

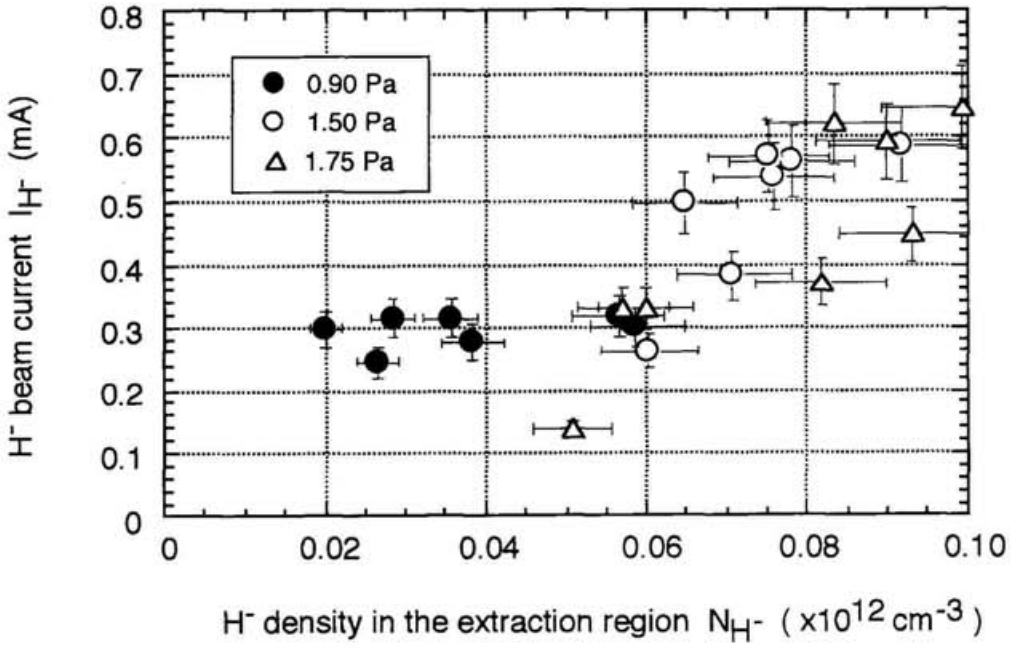

Fig. 5-1. The relation between the H^- density in the extraction region and the extracted H^- beam current at the operation without cesium.

is necessary in the driver region, high electron density is not always welcome in the extraction region. It is important to prevent high energy electrons from penetrating into extraction region. Comparing two types of magnetic filter field strength, as shown in section 4-2, it is found that the filter field need some strength enough to suppress high energy electrons. In the case of the ion source in this study, the strength of the configuration A is not sufficient .

From the gradient of the line in Fig. 5-1, the H^- temperature; T_{H^-} can be estimated if the H^- flux is conserved from the position of the probe in the extraction region to the surface of the plasma grid, as following expression[17];

$$J_{H^-} = \frac{1}{4} N_{H^-} e \left(\frac{8eT_{H^-}}{\pi M}\right)^{1/2} , \ (T_{H^-} \text{ in eV}) \qquad (5\text{-}1).$$

At 1.2 Pa of filling gas pressure, the H^- temperature is calculated as 0.3 eV. This is reasonable value for H^- ions in the plasma, compared with the measurement in other H^- sources[17][18][33].

5-2. Cesium effect

5-2-1. Ratio of the H^- beam current to the H^- density in the extraction region

After cesium vapor was injected into the arc chamber, the extracted H^- beam current

increased by twice, and the H^- density in the extraction region was remarkably enhanced by 5~10 times.

It is insufficient to explain the difference between the increasing ratio of the H^- density and that of the H^- beam current by enhancing the volume process in the extraction region, because the electron temperature in operation with cesium is not so lower than without cesium in this case. The contribution of processes (a) and (b) described in the section 2-3 is small.

Therefore another mechanism is necessary to explain the production of the large amount of H^- in the plasma after the cesium injection, in addition to the increase of the volume production of H^-. The cross-section of process (d) in the section 2-3 must be small enough for low temperature ions less than 1 eV. Therefore the surface production of H^- on the plasma grid; (c) in the section 2-3 is most probable.

In the arc chamber, the plasma grid is exposed to the heat flux by the radiation from the cathode filaments and by the electron bombardment from the plasma. In the case of this study, the temperature of the plasma grid arises up to about 300 °C on the discharge. Surface production efficiency of H^- has the proportional dependence on the plasma grid temperature as described in the section 2-3, so that it is supposed that good adsorption of cesium on the plasma grid is achieved during the arc discharge at this temperature.

Figure 5-2 shows the relation between the H^- density in the extraction region and the extracted H^- beam current. Using this relation, the H^- temperature is estimated by the same procedure with expression (5-1). In this case, the H^- temperature with the cesium injection resulted in considerably low value of 0.07 eV at 1.2 Pa. This temperature is much

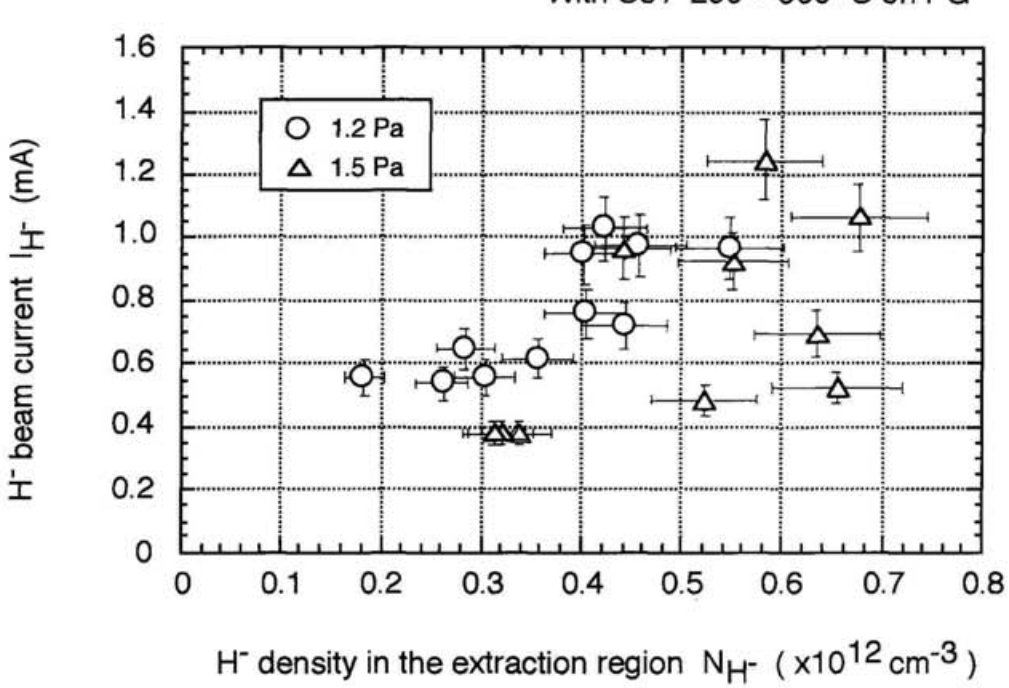

Fig. 5-2. The relation between the H^- density in the extraction region and the extracted H^- beam current at the operation with cesium.

lower than that in the operation without cesium.

Although the H^- temperature isn't actually measured in this source, I and collaborators have the other experimental results[34]. Ion temperature of the extraction region can be estimated by measuring the emittance of the extracted ion beam. If the emittance of a H^- beam; ε is known, the H^- temperature is estimated from following expression[35];

$$kT_{H^-} = \frac{\beta^2(1-\beta^2)^{-1} Mc^2\varepsilon^2}{4a^2} \qquad (5\text{-}2)$$

Here, c means the speed of light, $\beta = v/c$ (v means speed of the beam) M means rest mass of H^-, and a the radius of the beam. When I measure the emittance of the H^- beam with the 1/3-scale H^- source in NIFS, the 95 % emittance ε was 43.2 mm mrad when the filling gas pressure was 1.1 Pa, the discharge arc power was 35 kW, the beam energy was 87 kV and the extracted H^- beam current density was 10 mA/cm^2 [34]. At that time, the H^- temperature is calculated as 0.023 eV. This is very low temperature. Therefore 0.07 eV of the H^- energy estimated from the data in this section is supposed to be reasonable. It is considered that H^- ions on the laser path in the extraction region are almost relaxed with plasma including cesium ions whose temperature may be very low due to there large mass.

5-2-2. Returning processes of surface-produced H^-

Here, it is discussed how surface-produced H^- can return to the extraction aperture on the plasma grid. In our experimental condition, the plasma potential is at most about + 2 V against plasma grid and the wall of the arc chamber. In this situation, the produced H^- on the surface is accelerated by the plasma potential perpendicular to the surface. The acceleration energy is about 2 eV in our ion source. On the other hand, parallel velocity to the plasma grid is supposed to be much less than perpendicular velocity because the energy of the H^0 and H_n^+ in the plasma is low. Therefore, it is necessary to consider the process for H^- to return to the plasma grid in order to be extracted from the aperture on the plasma grid.

There are three possible processes to be considered[24].

(1) Mirror effect by the filter field.

(2) Elastic collisions with H^+ ions.

(3) Charge exchange with H^0.

The simplest process is the reflection directly by the mirror effect of the magnetic field on the extraction region. When the energy of an H^- ion is 2 eV, its Larmor radius is 25 mm at 0.0085 T (which is the field strength in the extraction region at configuration B) and is

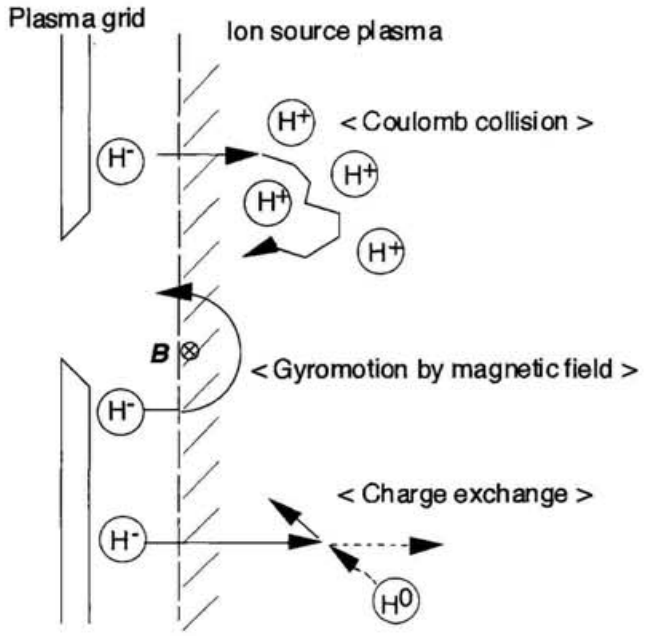

Fig. 5-3. An illustration of the models of the reflection of surface-produced H^- into an aperture on a plasma grid.

almost the same size with the depth of the external filter field. Then the surface- produced H^- can easily reach to the center part of the extraction region where I observe. But it doesn't contribute to the actual formation of H^- beam since surface H^- seems to be relaxed to lower temperature before extracted as a H^- beam. Surface-produced H^- is supposed to arrive in front of the extraction aperture after one or several collisions.

For examining whether the surface-produced H^- is relaxed like volume H^- before it reach on the extraction aperture through other processes, the mean free path (mfp) of the other processes is estimated. Here it is assumed that electron temperature $T_e \sim 0.4$ eV and the ion / atom temperature $T_H \sim 0.1$ eV. Electron density and ion density are assumed to be 1×10^{11} cm $^{-3}$. H^0 atom density is assumed to be 1×10^{12} cm^{-3} .

In considering the Coulomb collision as the process for surface-produced H^- to return to the plasma grid, it takes many collisions for relaxation with ions. Mfp for the Coulomb collision λ_{ii} is expressed as follows[36];

$$\lambda_{ii} = \frac{3^{1/2}\, 6\pi^{1/2} \varepsilon_0^{\,2} M^{1/2} T_e^{\,3/2}}{n_i e^4 \ln\Lambda} \left(\frac{3T_i}{M}\right)^{1/2} \tag{5-3}$$

Here, $\ln \Lambda$ is called Coulomb logarithm and approximated as follows[36];

$$\ln\Lambda \approx 7 + 2.3 \log_{10}\left\{ \left(\frac{T_e}{e}\right)^{3/2} \Big/ \left(\frac{n_e}{10^{20}}\right)^{1/2} \right\} \tag{5-4}$$

In the case of the assumption here, mfp for the Coulomb collision is calculated as about 6 cm. It is comparable to the Larmor radius.

The cross-section of the charge exchange

$$H^- + H^0 \rightarrow H^0 + H^- \qquad (5\text{-}5)$$

is about 1×10^{-14} cm^2 in the considered energy range of 2 eV[37]. Then mfp of the charge exchange is estimated as 1×10^3 cm. This mfp is much longer than the size of our ion source, so that the effect of the charge exchange is supposed to be much smaller than the other effects.

Next the mfp of the destruction process shown in the section 2-1 is described. Among the main destruction processes, the cross-section of mutual neutralization (2-5) is about 2×10^{-14} cm^2 in the considered energy region of 2 eV[38]. Then mfp of mutual neutralization is estimated as 5×10^2 cm. This is too large compared with the size of the arc chamber. If the energy of H^- is about 0.1 eV, the cross-section reaches about 2×10^{-13} cm, then mfp is estimated as 50 cm.

The cross-section of associative detachment (2-6) is about 10^{-14} cm^2[39]. If the ratio of H^0 to filling H_2 molecules is assumed to be few percents, H^0 densities are estimated as about 5×10^{12} cm^{-3}. Then the mfp of dissociative detachment is estimated to be 20 cm. This value is almost the same as the depth of the extraction region.

The cross-section of electron detachment (2-4) is estimated as 10^{-16} cm^2 in the considered energy region[40]. Then the mfp of electron detachment is estimated as 10^5 cm.

Process	cross section (cm^2)	mean free path (cm)
Coulomb collision		6
charge exchange	1×10^{-14}	1×10^{3}
mutual neutralization	2×10^{-14}	5×10^{2}
associative detachment	1×10^{-14}	20
electron detachment	1×10^{-16}	1×10^{5}
Larmor radius	2.5 cm	

Table 5-1. Estimated cross-sections and mean free paths of the processes in the extraction region.

Under this situation, it is supposed that a surface-produced H^-, which initially has high velocity perpendicular to the plasma grid, gyrate by the magnetic force of the filter field and is relaxed as a plasma particle through the collisional processes of the Coulomb collision with ions before the destructions by the collision. Then they extracted with the low temperature like a volume-produced H^-.

Cross-sections and mfp's estimated here are shown in table 5-1 for each discussed processes with the Larmor radius.

5-3. The effect of the bias voltage

Supply of bias voltage to the plasma grid with respect to the arc chamber caused the reduction of extracted electron and H^- beam current. At that time, H^- density in the extraction region shows the same dependence as H^- beam current, whereas electron density is independent to the bias voltage. It is considered from the independence of electrons in the extraction region that the effect of bias voltage to plasma is limited in very thin area faced on the plasma grid. Hence the bias voltage dependence of H^- suggest the exist of surface produced H^- because the plasma parameters in the extraction region are not affected by bias voltage. If the bias voltage is larger than the plasma potential, surface produced H^- cannot accelerated by the electric field between the plasma and the plasma grid and cannot reach into the plasma. Therefore the saturated value is considered as the component of volume produced H^-. As for the reduction of negative ions as the bias voltage in the case that bias voltage is smaller than plasma potential, the production efficiency on the surface is considered to be changed. If the dominant seed of H^- is H^+ from the plasma, its energy depends on the bias voltage because it is accelerated by sheath potential. The survival probability of H^- ion depends on its reflecting velocity so that the conversion efficiency from H^+ to H^- may be worse as the initial energy becomes low.

6. Conclusion

In order to consider the actual enhancement processes of H^- production in the high performance H^- source for N-NBI, the properties of the H^- beam extracted from the H^- source and the characteristics of the H^- density and electron density are measured and compared. Comparison are done in three cases of the techniques used for the general H^- sources for N-NBI; (1) effect of magnetic filter strength, (2) cesium injection into the arc chamber, and (3) supply of the bias voltage between the plasma grid and the arc chamber. As the results of comparison, the H^- density in the extraction region and the extracted H^- beam show strong correlation between them, whereas electrons show no correlation in some cases.

From observation of the effect of the external magnetic field strength on the extraction region, the H^- beam current can decreases at the higher arc power operation in the weak magnetic field. That is because the destruction of H^- in the extraction region exceeds the production of H^-. The weak magnetic field is insufficient to suppress the high energy electrons from the bulk plasma. From the comparison, it is concluded that magnetic field for the tandem H^- source must be strong not only enough to reduce the electron temperature less than 1 eV, as generally spoken, but also enough to suppress the high energy electrons which destruct H^- ions in the extraction region.

It is shown that effect of the cesium vapor injection into the arc chamber is huge, especially on the enhancement of the H^- density in the extraction region. The H^- beam

current is enhanced by about twice after the cesium injection. On the other hands, the H^- density in the extraction region surprisingly increase by 5~10 times. The difference in the increment ratio can be explained by the decrease of the H^- temperature after injection of cesium. The electron density and temperature do not change much when the cesium is injected. Therefore we don't think that the increase in H^- density is due to the enhancement of volume production processes.

Bias voltage has little influence on the electron density in the extraction region. But it has strong influence both on the extracted electron beam and on the H^- density and beam. Therefore, with regard to bias voltage, the H^- density in the extraction region does with the extracted H^- beam while the electron density at a distance of 15 mm from the plasma grid doesn't correlate with the extracted electron current.

In order to consider that the model of surface-produced H^- is reasonable, estimation is applied to the processes by which H^- shipped from the surface reaches at the grid aperture. If H^- with a speed perpendicular to the surface is supposed to go back to the surface, three processes are proposed. Two processes among them are reasonable because of their mean free paths; the one is concerned with Coulomb collision, another is by the magnetic mirror effect of filter field.

In order to construct the complete model of the surface production of H^-, the measurements is essential on hydrogen atom flux and positive hydrogen ion flux into the plasma grid surface. It is preferable to measure the density and the temperature of these particles in the extraction region, since they have important roles in the processes in the extraction region.

Acknowledgements

I would like to thank my thesis adviser Professor Osamu Kaneko for many suggestions and guidance through this work. I also would like to thank Professor Tsutomu Kuroda for encouragements and comments. Dr. I wish to thank Katsuyoshi Tsumori for his many useful discussions, suggestions and supervising in my course of experiments. I am also thankful to NBI group members at NIFS; Associate Professor Yasuhiko Takeiri, Dr. Yoshihide Oka, Dr. Masaki Osakabe, Mr. Eiji Asano, Mr. Toshikazu Kawamoto and Mr. Ryuichi Akiyama and former member, Dr. Toshihiko Takanashi for many comments, supports and very useful help. Without their support and encouragement, I could not have been completed this thesis.

I am indebted to Professor Samar Kumar Guharay for his collaboration and comments of H^- beam measurement at NIFS. I am deeply grateful to Professor Martha Bacal for her collaboration and guidance of the photodetachment method at NIFS. It was very delightful thing that I could have a precious time to discussion with the specialists of them in their fields.

References

[1] R. S. Hemsworth, J. H. Feist, M. Hanada, B. Heinemann, T. Inoue, E. Kussel, A. Krylov, P. Lotte, K. Miyamoto, N. Miyamoto, D. Murdoch, A. Nagase, Y. Ohara, Y. Okumura, J. Pamela, A. Panasenkov, K. Shibata, M. Tanii, and M. Watson, Rev. Sci. instrum, **67**, 1120 (1996)

[2] K. N. Berkner, R. V. Pyle, and J. W. Stearns, Nuclear Fusion **15**, 249 (1975).

[3] K. N. Leung, C. A. Haude, W. B. Kunkel, and A. R. Walther, Rev. Sci. Instrum. **60**, 531 (1989).

[4] Y. Okumura, M. Hanada, T. Inoue, H. Kojima, Y. Matsuda, Y. Ohara, M. Seki, and K. Watanabe, *Proc. of the 5th Int. Symp. on the Production and Neutralization of Negative Ions and Beams*, Brookhaven, NY, AIP Conf. Proc. No. 210 (1990)

[5] Y. Takeiri, O. Kaneko, Y. Oka, K. Tsumori, E. Asano, R. Akiyama, T. Kawamoto, T. Kuroda, and A. Ando, Rev. Sci, Instrum., **67**, 1021 (1996)

[6] K. Miyamoto, N. Akino, T. Aoyagi, N. Ebisawa, Y. Fujiwara, A. Honda, T. Inoue, T. Itoh, M. Kawai, M. Kazawa, J. Koizumi, M. Kuriyama, N. Miyamoto, K. Mogaki, Y. Ohara, T. Ohga, K. Ohshima, Y. Okumura, H Oohara, F. Satoh, K. Usui, K. Watanabe, M. Yamamoto, and T. Yamazaki, *Proc. of the 16th IAEA Fusion Energy Conference,* Montreal, (1996), IAEA-CN-64/GP-10.

[7] O. Kaneko, Y. Takeiri, K. Tsumori, Y. Oka, M. Osakabe, R. Akiyama, K. Kawamoto, E. Asano, and T. Kuroda, *Proc. of 16th IAEA Fusion Energy Conference*, Montreal (1996), IAEA-CN-64/GP-9.

[8] Y. Takeiri, A. Ando, O. Kaneko, Y. Oka, R. Akiyama, T. Kawamoto, A. Karita, K. Mineo, and T. Kuroda, *Proc of the 4th European Workshop of Production and Application of Light Negative Ions*, Belfast (1991) p. 78.

[9] Y. Takeiri, A. Ando, O. Kaneko, Y. Oka, K. Tsumori, R. Akiyama, E. Asano, T. Kawamoto, T. Kuroda, M. Tanaka, and H. Kawakami, Rev. Sci, Instrum., **66**, 2541 (1995)

[10] Y. Oka, K. Tsumori, Y. Takeiri, O. Kaneko, M. Osakabe, E. Asano, T. Kawamoto, and R. Akiyama, Rev. Sci. Instrum., **69**, 920(1998).

[11] M. Bacal, F. El Balghiti-Sube, L. T. Elizanov, and A. J. Tontegode, *Proc. of the 19th Symposium on Fusion Technology*, Portugal, 1996, North-Holland Amsterdam (1997)

[12] Y. Mori, T. Okuyama, A. Takagi, and D. Yuan, Nucl. Instrum. and Meth. in Phys. Res. **A301**, 1 (1991)

[13] K. N. Leung, K. W. Ehlers, and M. Bacal, Rev. Sci. Instrum. **54**, 56 (1983).

[14] T. Inoue, M. Araki, M. Hanada, T. Kurashima, S. Matsuda, Y. Ohara, Y. Okumura, S. Tanaka, and K. Watanabe, Nucl. Instrum. and Meth. in Phys. Res. **B37/38**, 111(1989).

[15] S. R. Walther, K. N. Leung, and W. B. Kunkel, J Appl. Phys., **64**, 3424 (1988).

[16] M. Bacal, F. Hillion, and M. Nachman, Rev. Sci. Instrum., **56**, 649 (1985), and M. Bacal, J. Brunetau, and P. Devynck, Rev. Sci. Instrum., **59**, 2152 (1988).

[17] M. Bacal and F. Hillion, Rev. Sci. Instrum, **56**, 2274 (1985).

[18] M. Bacal, P. Berlemont, A. M. Bruneteau, R. Leroy, and R. A. Stern, J. App. Phys. **70**, 1212 (1991), and C. Courteille, A. M. Bruneteau, and M. Bacal, Rev. Sci. Instrum., **66**, 2533 (1995).

[19] M. Bacal, A. M. Bruneteau, and M. Nachman, J. Appl. Phys., **55**, 15 (1983).

[20] J. R. Hiskes and A. M. Kara, Rev. Sci. Instrum., **56**, 1927 (1984).

[21] O. Fukumasa, J. Phys. D: appl. Phys. **22**, 1668 (1889).

[22] M. Ogasawara, R. Sakurai, T. Koshimine, S. Mitsuhashi, and A. Hatayama, Fusion Eng. and Design, **26**, 507 (1995).

[23] J. R. Hiskes and A. M. Karo, J. Appl. Phys. **56**, 1927 (1984).

[24] D. Riz and J. Pamela, *Proc. of 7th Int. Symp. Production and Neutralization of Negative Ions and Beams*, Upton, NY, 1995, AIP Conf. Proc. No. 380(1996) P. 3.

[25] M. Seidl, H. L. Cui, J. D. Isenberg, H. J. Kwon, and B. S. Lee, *Proc. 6thh Int. Symp. on Production and Neutralization of Negative Ions and Beams*, Upton, NY, 1992, AIP Conf. Proc. No. 287 (1994) p.25.

[26] Y. Mori, A. Takagi, K. Ikegami, and S. Fukumoto, *Proc. 4th Int. Symp. on Production and Neutralization of Negative Ions and Beams*, Brookhaven, NY, 1986, AIP Conf. Proc. No. 158 (1986) p.378.

[27] G. D. Alton and G. C. Blazey, Nucl. Instrum. and Meth. in Phys. Res., **166** 105 (1979).

[28] K. N. Leung, K. W. Ehlers, and R. V. Pyle, Rev. Sci. Instrum., **56**, 2097 (1985).

[29] M. Bacal, G. W. Hamilton, A. M. Bruneteau, H. J. Doucet, and J. Taillet, Rev. Sci. Instrum., **50**, 719 (1979).

[30] S. Geltman, Astrophys. J., **136**, 935 (1962).

[31] C. Michaut, M. Bacal, Yu. I. Belchenko, J. Auvray, C. Konieczny, and J. P. Stephan, Rev Sci Instrum., **65**, 1207 (1994).

[32] M. Hamabe, Y. Oka, K. Tsumori, T. Kuroda, and M. Bacal, Rev. Sci. Instrum., **69**, 1298 (1998)

[33] R. MacAdams, A. J. T. Holmes, and M. P. S. Nightingale, Rev. Sci. Instrum. **59**, 895 (1988).

[34] S. K. Guharay, K. Tsumori, M. Hamabe, Y. Takeiri, O. Kaneko, and T. Kuroda, Rev. Sci. Instrum., **67**, 2534 (1996).

[35] J. D. Lawson, *The Physics of Charged-Particle Beams*, 2nd edition (Oxford, New York, 1988) Chap. 4.

[36] K. Miyamoto, *The Plasma Phsics for Nuclear Fusion*, 2nd edition (in Japanese), (Iwanami, Tokyu, 1987) Chap.4.

[37] D. G. Hummer, R. F. Stebbings, W. L. Fite, and L. M. Branscomb, Phys. Rev. **119**, 668 (1960).

[38] D. Fussen and C. Kubach, J. Phys. B: At. Mol. Phys., **19**, L31, (1986).

[39] R. J. Bieniek, J. Phys. B: At. Mol. Phys., **13**, 4405 (1980).

[40] D. S. Walton, B. Peart, and K. T. Dolder, J. J. Phys. B: At. Mol. Phys., **4**,1343 (1971).